

Efficient Cluster-Based Catalysts for Asymmetric Hydrogenation of  $\alpha$ -Unsaturated Carboxylic AcidsViktor Moberg,<sup>[a]</sup> Robin Duquesne,<sup>[a]</sup> Simone Contaldi,<sup>[b]</sup> Oliver Röhrs,<sup>[a]</sup> Jonny Nachtigall,<sup>[a]</sup> Llewellyn Damoense,<sup>[c]</sup> Alan T. Hutton,<sup>[e]</sup> Michael Green,<sup>[c, d]</sup> Magda Monari,<sup>[b]</sup> Daniela Santelia,<sup>[f]</sup> Matti Haukka,<sup>[g]</sup> and Ebbe Nordlander\*<sup>[a]</sup>*In memory of John R. Moss*

**Abstract:** The new clusters  $[\text{H}_4\text{Ru}_4(\text{CO})_{10}(\mu\text{-}1,2\text{-P-P})]$ ,  $[\text{H}_4\text{Ru}_4(\text{CO})_{10}(1,1\text{-P-P})]$  and  $[\text{H}_4\text{Ru}_4(\text{CO})_{11}(\text{P-P})]$  (P-P = chiral diphosphine of the ferrocene-based Josiphos or Walphos ligand families) have been synthesised and characterised. The crystal and molecular structures of eleven clusters reveal that the coordination modes of the diphosphine in the  $[\text{H}_4\text{Ru}_4(\text{CO})_{10}(\mu\text{-}1,2\text{-P-P})]$  clusters are different for the Josiphos and the Walphos ligands. The Josiphos ligands bridge a metal–metal bond of the ruthenium tetrahedron in the “conventional” manner, that is, with both phosphine moieties coordinated in equatorial positions relative to a triangular face of the tetrahedron, whereas the phosphine moieties of the Walphos ligands coordinate in one axial and one equatorial position. The differences in the ligand size and the coordination mode

between the two types of ligands appear to be reflected in a relative propensity for isomerisation; in solution, the  $[\text{H}_4\text{Ru}_4(\text{CO})_{10}(1,1\text{-Walphos})]$  clusters isomerise to the corresponding  $[\text{H}_4\text{Ru}_4(\text{CO})_{10}(\mu\text{-}1,2\text{-Walphos})]$  clusters, whereas the Josiphos-containing clusters show no tendency to isomerisation in solution. The clusters have been tested as catalysts for asymmetric hydrogenation of four prochiral  $\alpha$ -unsaturated carboxylic acids and the prochiral methyl ester (*E*)-methyl 2-methylbut-2-enoate. High conversion rates (> 94 %) and selectivities of product formation were observed for almost all catalysts/catalyst precursors. The observed enantioselectivities were low or nonexistent

for the Josiphos-containing clusters and catalyst (cluster) recovery was low, suggesting that cluster fragmentation takes place. On the other hand, excellent conversion rates (99–100 %), product selectivities (99–100 % in most cases) and good enantioselectivities, reaching 90 % enantiomeric excess (*ee*) in certain cases, were observed for the Walphos-containing clusters, and the clusters could be recovered in good yield after completed catalysis. Results from high-pressure NMR and IR studies, catalyst poisoning tests and comparison of catalytic properties of two  $[\text{H}_4\text{Ru}_4(\text{CO})_{10}(\mu\text{-}1,2\text{-P-P})]$  clusters (P-P = Walphos ligands) with the analogous mononuclear catalysts  $[\text{Ru}(\text{P-P})(\text{carboxylato})_2]$  suggest that these clusters may be the active catalytic species, or direct precursors of an active catalytic cluster species.

**Keywords:** asymmetric catalysis · cluster compounds · hydrogenation · ruthenium

[a] Dr. V. Moberg, R. Duquesne, O. Röhrs, J. Nachtigall, Dr. E. Nordlander  
Inorganic Chemistry Research Group, Chemical Physics  
Center for Chemistry and Chemical Engineering  
Lund University  
Box 124, 221 00 Lund (Sweden)  
Fax: (+46)46-222-0310  
E-mail: Ebbe.Nordlander@chemphys.lu.se

[b] Dr. S. Contaldi, Prof. M. Monari  
Dipartimento di Chimica “G. Ciamician”  
Università degli Studi di Bologna  
Via Selmi 2, 40126 Bologna (Italy)

[c] L. Damoense, Dr. M. Green  
Sasol Technology  
1 Klasie Havenga Road, Sasolburg  
1947 (South Africa)

[d] Dr. M. Green  
Present address: School of Chemistry  
Newcastle University  
Newcastle upon Tyne, NE1 7RU (UK)

[e] Dr. A. T. Hutton  
Department of Chemistry  
University of Cape Town  
Private Bag, Rondebosch 7701 (South Africa)

[f] D. Santelia  
Dipartimento di Chimica I.F.M.  
Università di Torino  
Via P. Giuria 7, 10125 Torino (Italy)

[g] Prof. M. Haukka  
Department of Chemistry  
University of Eastern Finland  
Box 111, 80101 Joensuu (Finland)

 Supporting information for this article is available on the WWW under <http://dx.doi.org/10.1002/chem.201200630>.

## Introduction

During the past 40 years there has been a tremendous development in homogeneous-catalysed enantioselective hydrogenation and a large number of new chiral ligands and catalysts has been developed for this type of reaction.<sup>[1,2]</sup> Asymmetric hydrogenation reactions are predominantly catalysed by either ruthenium- or rhodium-based catalysts.<sup>[3]</sup> Enantioselectivities have been found to be dependent on the substrate used<sup>[3]</sup> and the most frequently reported results for asymmetric hydrogenation where high enantioselectivities are obtained involve substrates such as unsaturated carboxylic acids with  $\alpha$ -acylamido groups.<sup>[1,3,4]</sup>

There has been a considerable interest in the use of transition-metal carbonyl clusters as catalysts for various chemical reactions of industrial relevance<sup>[5,6]</sup> but very few studies have been carried out on the potential of clusters to act as catalysts for asymmetric synthesis. In similarity to pure heterogeneous catalysts, transition-metal carbonyl clusters are often thermally stable and the presence of more than one metal in a catalyst offers, in principle, the opportunity of new pathways for the activation of molecules and the regioselectivity in reactions due to differentiated metal binding of a substrate molecule (reactant).<sup>[7]</sup> It has indeed been found that metal carbonyl clusters can function as efficient catalysts (or catalyst precursors) for several diverse chemical reactions,<sup>[5]</sup> but cluster-based catalysis has not yet proven to be commercially viable.

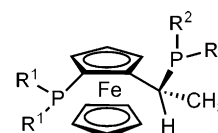
It has been demonstrated that hydride-containing trinuclear and tetranuclear ruthenium carbonyl cluster anions are effective catalysts/catalyst precursors for hydroformylation,<sup>[8]</sup> hydrosilylation<sup>[9]</sup> and reductive coupling<sup>[10]</sup> reactions as well as the water-gas shift reaction.<sup>[11]</sup> In pioneering systematic studies, Matteoli and co-workers have shown that clusters of the general formula  $[\text{H}_4\text{Ru}_4(\text{CO})_{12-2x}(\text{P-P})_x]$  ( $x=1,2$ ; P-P = chiral diphosphine) are good catalysts for asymmetric isomerisation,<sup>[12]</sup> hydroformylation<sup>[13]</sup> and hydrogenation reactions.<sup>[14]</sup>

The best enantiomeric excesses (*ees*) hitherto reported for cluster-based asymmetric catalysis are approximately 45% in the case of hydrogenation of tiglic acid ((*E*)-2-methyl-2-butenic acid) by the diphosphine-derivatised cluster  $[\text{H}_4\text{Ru}_4(\text{CO})_{10}(1,1\text{-bdpp})]$  (bdpp = (2*R*/*S*,4*R*/*S*)-2,4-bis(diphenylphosphino)pentane).<sup>[15]</sup> In contrast to previous attempts in cluster-based (asymmetric) hydrogenation<sup>[14]</sup> the catalysis was found to take place under relatively mild reaction conditions. It was observed that a strong chiral induction was indirectly shown by the fact that the chirality of the predominating enantiomer of the product (2-methylbutyric acid) was dependent on the chirality of the bdpp ligand.<sup>[15]</sup>

The use of ferrocene-based chiral ligands in homogeneous asymmetric synthesis has proven to be highly efficient in conjunction with single-site transition-metal catalysts based on cobalt, rhodium, iridium and ruthenium.<sup>[16]</sup> Several members of the Solvias ligand families have been successfully employed with  $\text{Rh}^I$ ,  $\text{Ir}^I$  and  $\text{Pd}^{II}$  complexes to catalyse enantioselective reactions on both laboratory and industrial

scale.<sup>[1,17,18]</sup> Here, we demonstrate the importance of the chiral ligand for enantioselective cluster-based catalysis. The use of tetraruthenium cluster catalysts of the type  $[\text{H}_4\text{Ru}_4(\text{CO})_{10}(\text{P-P})]$  containing ferrocene-based ligands from the chiral Josiphos- and Walphos-diphosphine families<sup>[19]</sup> (Tables 1 and 2) has led to unparalleled catalytic activities for cluster-based catalysis, exhibiting both high conversion rates and enantiomeric excesses exceeding 90% in the hydrogenation of prochiral  $\alpha$ -unsaturated carboxylic acids. Parts of these results have been published in an earlier communication.<sup>[20]</sup>

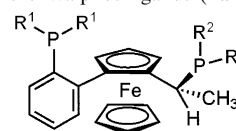
Table 1. Structures of the Josiphos ligands (**1a–1d**) used in this investigation.



Ligand	R <sup>1</sup>	R <sup>2</sup>
<b>1a</b>	Ph	Cy <sup>[a]</sup>
<b>1b</b>	Ph	<i>t</i> Bu
<b>1c</b>	Cy	Cy
<b>1d</b>	Ph	3,5-(CH <sub>3</sub> ) <sub>2</sub> C <sub>6</sub> H <sub>3</sub>

[a] Cy = cyclohexyl.

Table 2. Structures of the Walphos ligands (**2a–2g**) used in this report.



Ligand	R <sup>1</sup>	R <sup>2</sup>
<b>2a</b>	Ph	3,5-(CF <sub>3</sub> ) <sub>2</sub> C <sub>6</sub> H <sub>3</sub>
<b>2b</b>	Ph	Ph
<b>2c</b>	Ph	Cy
<b>2d</b>	3,5-(CH <sub>3</sub> ) <sub>2</sub> -4-(CH <sub>3</sub> O)C <sub>6</sub> H <sub>2</sub>	3,5-(CF <sub>3</sub> ) <sub>2</sub> C <sub>6</sub> H <sub>3</sub>
<b>2e</b>	Ph	3,5-(CH <sub>3</sub> ) <sub>2</sub> C <sub>6</sub> H <sub>3</sub>
<b>2f</b>	Cy	3,5-(CF <sub>3</sub> ) <sub>2</sub> C <sub>6</sub> H <sub>3</sub>
<b>2g</b>	3,5-(CH <sub>3</sub> ) <sub>2</sub> C <sub>6</sub> H <sub>3</sub>	3,5-(CH <sub>3</sub> ) <sub>2</sub> C <sub>6</sub> H <sub>3</sub>

## Results and Discussion

The syntheses of the chiral diphosphine derivatives of  $[\text{H}_4\text{Ru}_4(\text{CO})_{12}]$  were based on previously published methods,<sup>[15,21]</sup> that is, either 1) oxidative decarbonylation (by using  $\text{Me}_3\text{NO}$ ) in the presence of the diphosphine in a benzene/methanol solution at ambient temperature or heating to reflux, or 2) thermal substitution in benzene under elevated pressures of hydrogen gas (25–30 bar). The latter method was found to be superior with respect to yield and selectivity in product formation. The clusters were identified by IR, <sup>1</sup>H and <sup>31</sup>P NMR spectroscopy, mass spectrometry and, wherever possible, X-ray crystallography.

**Synthesis and characterisation of tetraruthenium clusters containing the Josiphos ligands 1a–1d:** The preparation of

clusters containing ligands **1a–1d** was carried out by oxidative decarbonylation of  $[\text{H}_4\text{Ru}_4(\text{CO})_{12}]$  by using  $\text{Me}_3\text{NO}$  as the decarbonylation reagent (see the Experimental Section and the Supporting Information). For each diphosphine, the two isomers of  $[\text{H}_4\text{Ru}_4(\text{CO})_{10}(\text{P-P})]$  in which the diphosphine either chelates one ruthenium atom ( $[\text{H}_4\text{Ru}_4(\text{CO})_{10}(1,1\text{-P-P})]$ ) or bridges one Ru–Ru edge ( $[\text{H}_4\text{Ru}_4(\text{CO})_{10}(\mu\text{-}1,2\text{-P-P})]$ ) were isolated (Table 3), with the latter isomer

Table 3. A summary of cluster compounds and phosphine coordination modes found in this study. See Tables 1 and 2 for structures of the ligands. Note the difference in coordination for bridging Josiphos versus Walphos ligands (see text).

$[\text{H}_4\text{Ru}_4(\text{CO})_{11,2\text{a}}]$ ( <b>13</b> )	$[\text{H}_4\text{Ru}_4(\text{CO})_{10}(\mu\text{-}1,2\text{-1a})]$ ( <b>4</b> )	$[\text{H}_4\text{Ru}_4(\text{CO})_{10}(1,1\text{-1a})]$ ( <b>3</b> )
	$[\text{H}_4\text{Ru}_4(\text{CO})_{10}(\mu\text{-}1,2\text{-1b})]$ ( <b>6</b> )	$[\text{H}_4\text{Ru}_4(\text{CO})_{10}(1,1\text{-1b})]$ ( <b>5</b> )
	$[\text{H}_4\text{Ru}_4(\text{CO})_{10}(\mu\text{-}1,2\text{-1c})]$ ( <b>8</b> )	$[\text{H}_4\text{Ru}_4(\text{CO})_{10}(1,1\text{-1c})]$ ( <b>7</b> )
	$[\text{H}_4\text{Ru}_4(\text{CO})_{10}(\mu\text{-}1,2\text{-1d})]$ ( <b>10</b> )	$[\text{H}_4\text{Ru}_4(\text{CO})_{10}(1,1\text{-1d})]$ ( <b>9</b> )
	$[\text{H}_4\text{Ru}_4(\text{CO})_{10}(\mu\text{-}1,2\text{-2a})]$ ( <b>12</b> )	$[\text{H}_4\text{Ru}_4(\text{CO})_{10}(1,1\text{-2a})]$ ( <b>11</b> )
	$[\text{H}_4\text{Ru}_4(\text{CO})_{10}(\mu\text{-}1,2\text{-2b})]$ ( <b>15</b> )	$[\text{H}_4\text{Ru}_4(\text{CO})_{10}(1,1\text{-2b})]$ ( <b>14</b> )
	$[\text{H}_4\text{Ru}_4(\text{CO})_{10}(\mu\text{-}1,2\text{-2c})]$ ( <b>17</b> )	$[\text{H}_4\text{Ru}_4(\text{CO})_{10}(1,1\text{-2c})]$ ( <b>16</b> )
	$[\text{H}_4\text{Ru}_4(\text{CO})_{10}(\mu\text{-}1,2\text{-2d})]$ ( <b>18</b> )	
	$[\text{H}_4\text{Ru}_4(\text{CO})_{10}(\mu\text{-}1,2\text{-2e})]$ ( <b>19</b> )	
	$[\text{H}_4\text{Ru}_4(\text{CO})_{10}(\mu\text{-}1,2\text{-2f})]$ ( <b>20</b> )	
	$[\text{H}_4\text{Ru}_4(\text{CO})_{10}(\mu\text{-}1,2\text{-2g})]$ ( <b>21</b> )	

being the predominant product. The isomers were identified on the basis of comparison of their IR spectra to those of the corresponding isomers of related  $[\text{H}_4\text{Ru}_4(\text{CO})_{10}(\text{P-P})]$  clusters<sup>[15,21–23]</sup> and in the cases of clusters **4** and **7–9**, their structures (in the solid state) were corroborated by X-ray crystallography. Attempts to affect the product distribution between the chelating and the bridging isomers by varying the reaction temperature (0–70 °C) did not have any notable effects. However, in the case of ligand **1c** it was found that an autoclave reaction of  $[\text{H}_4\text{Ru}_4(\text{CO})_{12}]$  with the diphosphine at 125 °C and 30 bar of  $\text{H}_2$  gave exclusively the bridging isomer **8**. It has previously been shown that  $[\text{H}_4\text{Ru}_4(\text{CO})_{10}(\mu\text{-}1,2\text{-P-P})]$  isomers—for example, P-P = dppe,<sup>[24]</sup> bdpp ((2*R*/*S*,4*R*/*S*)-2,4-bis(diphenylphosphino)pentane),<sup>[15]</sup> BINAP (2,2'-bis(diphenylphosphino)-1,1'-binaphthyl),<sup>[22]</sup> or DIPAMP (ethane-1,2-diylbis[(2-methoxyphenyl)phenylphosphane])<sup>[21]</sup>—can rearrange to form the corresponding  $[\text{H}_4\text{Ru}_4(\text{CO})_{10}(1,1\text{-P-P})]$  isomers. In contrast to the corresponding clusters containing the Walphos ligands **2a–2g** (see below), none of clusters **3–10** containing the Josiphos ligands **1a–1d** showed any propensity towards isomerisation.

### Crystal and molecular structures of clusters **4** and **7–9**

**General description of the molecular structures:** The clusters contain pseudo-tetrahedral  $\text{H}_4\text{Ru}_4$  cores. The arrangement of the four hydrides yields an  $\text{H}_4\text{Ru}_4$  cluster core with  $C_s$  symmetry, rather than  $D_{2d}$  as observed for the parent cluster

$[\text{H}_4\text{Ru}_4(\text{CO})_{12}]$  and for the bis-phosphine-derivatised clusters  $[\text{H}_4\text{Ru}_4(\text{CO})_{10}(\text{NMDPP})_2]$ <sup>[21]</sup> and  $[\text{H}_4\text{Ru}_4(\text{CO})_{10}(\text{PPh}_3)_2]$ .<sup>[25]</sup> The  $C_s$  symmetry found in the  $\text{H}_4\text{Ru}_4$  core seems to be a common feature shared by  $[\text{H}_4\text{Ru}_4(\text{CO})_{10}(\text{diphosphine})]$  clusters and has been reported for both chelating<sup>[15]</sup> and bridging<sup>[15,21,24]</sup> coordination modes of the diphosphine ligands. All four hydrides coordinate at least to one of the ruthenium atoms that are coordinated to the phosphorus moieties of the ligand. The Ru–Ru bond lengths are divided into two distinctive classes—the four hydrido-bridged Ru–Ru bonds are “long” and the two non-bridged Ru–Ru bonds are “short”. All CO ligands are bound in a terminal monodentate coordination mode and are staggered with respect to the Ru–Ru vectors, in contrast to the eclipsed conformation of the carbonyls in  $[\text{H}_4\text{Re}_4(\text{CO})_{12}]$ , where each of the four hydrides bridges a triangular metal face.<sup>[25]</sup>

### Molecular structure of $[\text{H}_4\text{Ru}_4(\text{CO})_{10}(\mu\text{-}1,2\text{-1a})]$ (**4**):

The molecular structure of cluster **4** is shown in Figure 1 and relevant bond lengths and angles are presented in Table 4. Ligand **1a** bridges one Ru–Ru edge giving rise to a seven-membered dimetallacycle and the  $\text{H}_4\text{Ru}_4$  core conforms to a  $C_s$  symmetry as found in other  $[\text{H}_4\text{Ru}_4(\text{CO})_{10}(\text{P-P})]$  clusters. There are two short ( $\text{Ru–Ru}_{\text{average}} = 2.784 \text{ \AA}$ ) and four long ( $\text{Ru–Ru}_{\text{average}} = 2.973 \text{ \AA}$ ) intermetallic distances, where the latter are related to the hydride-bridged Ru–Ru vectors (see above). This trend is typical for diphosphine-substituted  $[\text{H}_4\text{Ru}_4(\text{CO})_{12}]$  derivatives, and similar elongation of the Ru–Ru bonds bridged by the hydride ligands was observed in other  $[\text{H}_4\text{Ru}_4(\text{CO})_{10}(\text{diphosphine})]$  clusters, such as  $[\text{H}_4\text{Ru}_4(\text{CO})_{10}(\mu\text{-}1,2\text{-bdpp})]$ ,<sup>[15]</sup>  $[\text{H}_4\text{Ru}_4(\text{CO})_{10}(\mu\text{-}1,2\text{-DIOP})]$ <sup>[21]</sup> (DIOP = (4*R*,5*R*)-2,2-dimethyl-4,5-bis[(diphenylphosphino)methylene]-1,3-dioxolane) and  $[\text{H}_4\text{Ru}_4(\text{CO})_{10}(\mu\text{-}1,2\text{-dppe})]$ .<sup>[24]</sup>

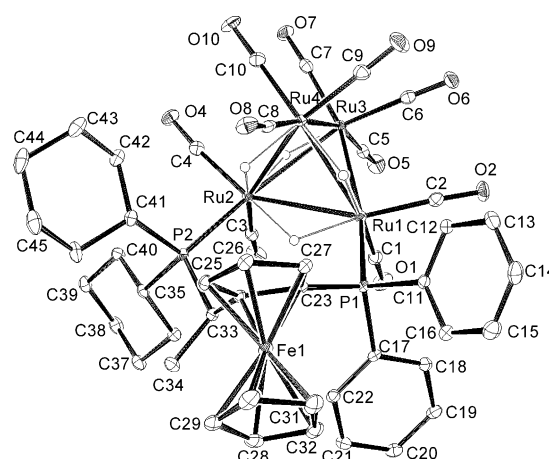


Figure 1. ORTEP drawing of the molecular structure of  $[\text{H}_4\text{Ru}_4(\text{CO})_{10}(\mu\text{-}1,2\text{-1a})]$  (**4**). Thermal ellipsoids are drawn at the 30% probability level. For the sake of clarity, all hydrogen atoms except the hydrides have been omitted.

Table 4. Selected bond lengths [Å] and angles [°] for clusters **4** and **7–9**.

	<b>4</b>	<b>7</b>	<b>8</b>	<b>9</b>
Ru1–Ru2	2.9656(3) <sup>[a]</sup>	2.9776(3) <sup>[a]</sup>	2.9768(3) <sup>[a]</sup>	2.9961(3) <sup>[a]</sup>
Ru1–Ru3	2.7750(3)	3.0238(3) <sup>[a]</sup>	2.7976(3)	2.9580(3) <sup>[a]</sup>
Ru1–Ru4	2.9544(3) <sup>[a]</sup>	3.0940(2) <sup>[a]</sup>	2.9620(4) <sup>[a]</sup>	3.0320(3) <sup>[a]</sup>
Ru2–Ru3	2.9812(3) <sup>[a]</sup>	2.7785(3)	2.9860(3) <sup>[a]</sup>	2.7922(3)
Ru2–Ru4	2.9900(3) <sup>[a]</sup>	2.7823(3)	2.9686(3) <sup>[a]</sup>	2.9288(3) <sup>[a]</sup>
Ru3–Ru4	2.7932(3)	2.9289(2) <sup>[a]</sup>	2.7815(3)	2.7890(3)
Ru1–P1	2.3418(7)	2.4020(6)	2.3655(7)	2.3261(7)
Ru2–P2	2.3760(7)		2.3594(7)	
Ru1–P2		2.3550(6)		2.3148(6)
P1–Ru1–Ru2	109.52(2)		113.824(19)	
P...P <sup>[b]</sup>	4.644	3.492	4.617	3.199
P2–Ru2–Ru1	112.104(18)		106.706(19)	
P1–Ru1–Ru2–P2	3.05(3)		6.02(3)	
P2–Ru1–P1		92.233(18)		87.14(2)

[a] Ru–Ru bond bridged by hydride. [b] Measured with the Mercury software (<http://www.ccdc.cam.ac.uk/products/mercury/>).

The two phosphorus atoms are coordinated in the same relative positions on a triangular face of the  $[H_4Ru_4(CO)_{12}]$  framework, as seen for other diphosphine derivatives of  $H_4Ru_4$  clusters.<sup>[15,21,24]</sup> The Ru–P bond lengths in **4** are also similar to those observed for  $H_4Ru_4$ -phosphine derivatives,<sup>[15,21]</sup> but are notably asymmetric, 2.3418(7) (Ru1–P1) and 2.3760(7) Å (Ru2–P2). Such a variation is not unprecedented in this type of cluster, but it may be related to the relative  $\pi$ -acceptor ability of each phosphine moiety, which is affected by the phosphorus substituents. Thus, the aryl substituents on P1 are expected to make it a slightly better  $\pi$  acceptor than P2. The P...P separation in **4** (4.644 Å) is in the range observed for the seven-membered “dimetallacycles” in  $[H_4Ru_4(CO)_{10}-\mu-1,2-DIOP]^{[21]}$  (4.870 Å) and  $[H_4Ru_4(CO)_{10}-\mu-1,2-bdpp]^{[15]}$  (4.536 Å).

**Molecular structure of  $[H_4Ru_4(CO)_{10}(1,1-Ic)]$  (**7**):** The molecular structure of cluster **7** is shown in Figure 2 and bond lengths and angles are summarised in Table 4. The coordinated ligand **1c** is chelating the ruthenium atom that is connected to three hydrides and forms a six-membered ring. The  $H_4Ru_4$  core conforms to  $C_s$  symmetry with four long ( $Ru-Ru_{average} = 3.006$  Å) and two short ( $Ru-Ru_{average} = 2.780$  Å) metal–metal distances. The two Ru–P bond lengths (Ru1–P1 = 2.402, Ru1–P2 = 2.355 Å) are asymmetric and somewhat longer than the corresponding distances in cluster **4**. The bite angle (P2–Ru1–P1) generated by the ligand is 92.23°, which is similar to that observed for  $[H_4Ru_4(CO)_{10}(1,1-bdpp)]$  ( $\approx 91.85^\circ$ ).<sup>[15]</sup>

**Molecular structure of  $[H_4Ru_4(CO)_{10}(\mu-1,2-Ic)]$  (**8**):** For cluster **8**, the molecular structure is shown in Figure 3 (bond lengths and angles are reported in Table 4). The  $H_4Ru_4$  core conforms to  $C_s$  symmetry. The bridging coordinated diphosphine ligand **1c** generates a seven-membered ring, similar to that in cluster **4**, with the same relative positions of the two different phosphine moieties. The lengths of the Ru vectors follow the same pattern as reported for other  $[H_4Ru_4(CO)_{10}-(P-P)]$  clusters, that is, two “short” and four “long” distances

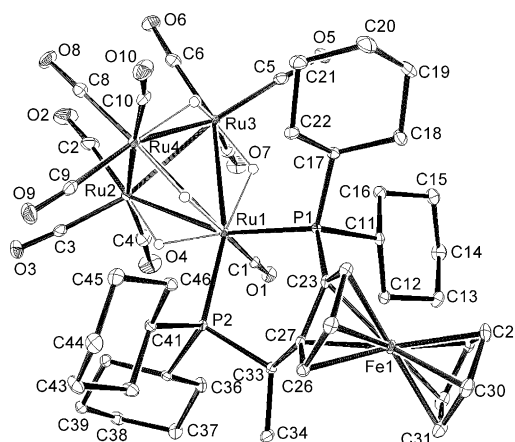


Figure 2. ORTEP drawing of the molecular structure of  $[H_4Ru_4(CO)_{10}(1,1-Ic)]$  (**7**). Thermal ellipsoids are drawn at the 30% probability level. For the sake of clarity, all hydrogen atoms except the hydrides have been omitted.

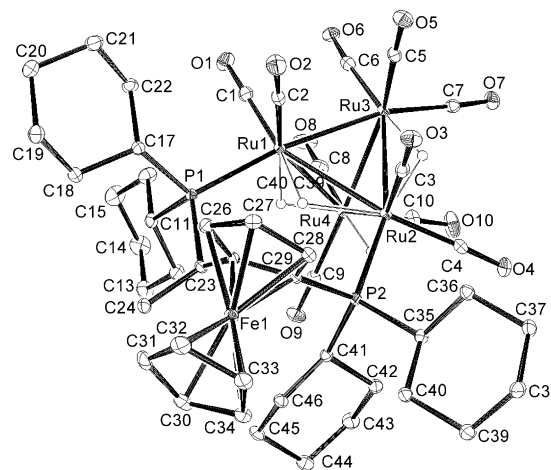


Figure 3. ORTEP drawing of the molecular structure of  $[H_4Ru_4(CO)_{10}(\mu-1,2-Ic)]$  (**8**). Thermal ellipsoids are drawn at the 30% probability level. For the sake of clarity, all hydrogen atoms except the hydrides have been omitted.

( $Ru-Ru_{average} = 2.789$  and  $Ru-Ru_{average} = 2.973$  Å, respectively). The two Ru–P distances differ only very slightly (Ru1–P1 = 2.3655(7) and Ru2–P2 = 2.3594(7) Å), with the shortest Ru–P distance being that of the non-chiral arm of the ligand, as previously noted for clusters **4** and **7**.

**Molecular structure of  $[H_4Ru_4(CO)_{10}(1,1-Id)]$  (**9**):** The molecular structure of cluster **9** is shown in Figure 4 (see Table 4 for relevant bond lengths and angles). The ligand **1d** chelates the ruthenium atom that is coordinated by three bridging hydrides and forms a six-membered ring. The  $H_4Ru_4$  cluster core adapts to  $C_s$  symmetry with four long ( $Ru-Ru_{average} = 2.978$  Å) and two short ( $Ru-Ru_{average} = 2.791$  Å) metal–metal distances. The bite angle P2–Ru1–P1 (87.14°) is notably smaller than that observed for the cluster **7**. The two Ru–P distances, Ru1–P1 and Ru1–P2, are approximately equal, 2.326 and 2.315 Å (within the estimated

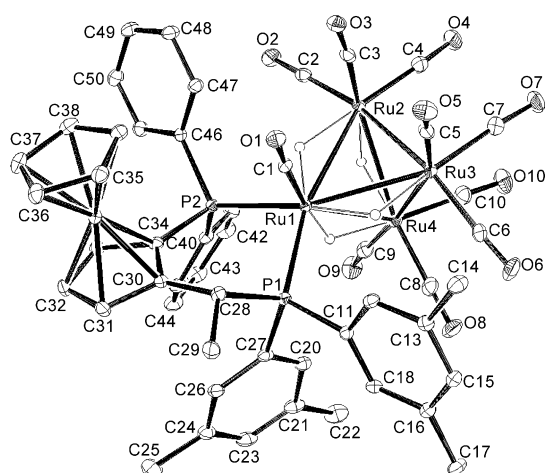


Figure 4. ORTEP drawing of the molecular structure of  $[\text{H}_4\text{Ru}_4(\text{CO})_{10}(1,1\text{-1d})]$  (**9**). Thermal ellipsoids are drawn at the 30% probability level. For the sake of clarity, all hydrogen atoms except the hydrides have been omitted.

standard deviation), respectively—significantly shorter than those found for cluster **7** and  $[\text{H}_4\text{Ru}_4(\text{CO})_{10}\{1,1\text{-}(S,S \text{ or } R,R)\text{-bdpp}\}]^{[15]}$  ( $\approx 2.34 \text{ \AA}$ ). As noted above for clusters **4**, **7** and **8**, the slightly shorter Ru–P bond length is located at the non-chiral arm of the ligand.

**Synthesis and characterisation of tetraruthenium clusters containing the Walphos ligands 2a–2g:** The ligand framework of the Walphos ligands **2a–2g** differs from that of the Josiphos ligands **1a–1d** by the insertion of a benzyl moiety into the nonchiral phosphine “arm” of the ligand (see Table 2). There is thus a six-bond P⋯P separation in ligands **2a–2g** as opposed to a four-bond separation in **1a–1d**; the inherent “bite” of the Walphos ligands is therefore considerably wider than that of the Josiphos ligands and—as will be shown below—this has repercussions on both the structures and the dynamics of the Walphos-containing tetraruthenium clusters **10–21**.

The two synthetic methods used to prepare clusters containing the ligands **1a–1d** (see above) were also employed for the synthesis of clusters with ligands **2a–2g**. Although the yields obtained for each isolated cluster differ, the observed general trend is that the thermal substitution reaction method is superior to oxidative decarbonylation in terms of yield. For ligand **2a**, the products  $[\text{H}_4\text{Ru}_4(\text{CO})_{10}(1,1\text{-2a})]$  (**11**, 7%),  $[\text{H}_4\text{Ru}_4(\text{CO})_{10}(\mu\text{-1,2-2a})]$  (**12**, 43%) and  $[\text{H}_4\text{Ru}_4(\text{CO})_{11}(\mathbf{2a})]$  (**13**, 44%) were isolated when the oxidative decarbonylation method was used. By varying the reaction time and the amount of  $\text{Me}_3\text{NO}$  added to the reaction mixture, relatively high yields (44%) of the cluster “intermediate” **13**, in which the diphosphine coordinates as a monodentate ligand through the nonchiral arm, were obtained. On the other hand, cluster **11** could only be isolated in very small quantities, but the yield was slightly improved when an excess of the ligand was added to the reaction mixture. Thermal ligand substitution led to the formation of **12** in good yield (73%), as the only isolated product.

The empirical formulae of clusters **11–21** were confirmed by mass spectrometry, and their structures in solution and the solid state were identified by IR and NMR spectroscopy, as well as X-ray crystallography in certain cases. The IR spectrum of **12** suggested that the overall structure of the cluster was not identical to that already established for the analogous  $[\text{H}_4\text{Ru}_4(\text{CO})_{10}(\mu\text{-1,2-Josiphos})]$  clusters **4**, **6**, **8** and **10** (see above), but it resembled the IR spectrum of clusters **3**, **5**, **7** and **9**, suggesting that the structure of **12** is analogous to these four clusters with respect to the relative orientation of the phosphine moieties on the tetraruthenium cluster framework. The crystal structure of **12** (see below) confirmed that this was the case. Comparison of the IR spectra of **11** and **12** to those of the analogous  $[\text{H}_4\text{Ru}_4(\text{CO})_{11}(\text{PR}_3)]^{[21]}$  and  $[\text{H}_4\text{Ru}_4(\text{CO})_{10}(1,1\text{-P-P})]^{[15,22]}$  clusters, respectively, indicated their structures and in the case of **13** the (solid-state) structure could be corroborated by a crystal structure determination.

Although the hydrides in the parent cluster  $[\text{H}_4\text{Ru}_4(\text{CO})_{12}]$  and most of its (phosphine) derivatives usually exhibit complete fluxionality at ambient temperature, four relatively sharp resonances could be detected for the hydrides in the  $^1\text{H}$  NMR spectra of **11** and **12**. Variable-temperature (VT)  $^1\text{H}$  NMR spectra recorded for cluster **12** show that the four hydrides are static at 273 K (Figure 5) and that complete fluxionality is not achieved even at 383 K (Figure 6). The hydride resonances in cluster **12** could be assigned on the basis of its crystal structure, COSY and EXSY (exchange spectroscopy) spectra (Figures 7 and 8), a  $^{31}\text{P}$  NMR spectrum,  $^1\text{H}$ ,  $^{31}\text{P}$  coupling constants and a  $^1\text{H}$ ,  $^{31}\text{P}$  HetCor spectrum (Figure 9). As may be expected, it was found that the hydride  $\text{H}^e$  located in between the two phosphines, as demonstrated by its correlation peaks with both

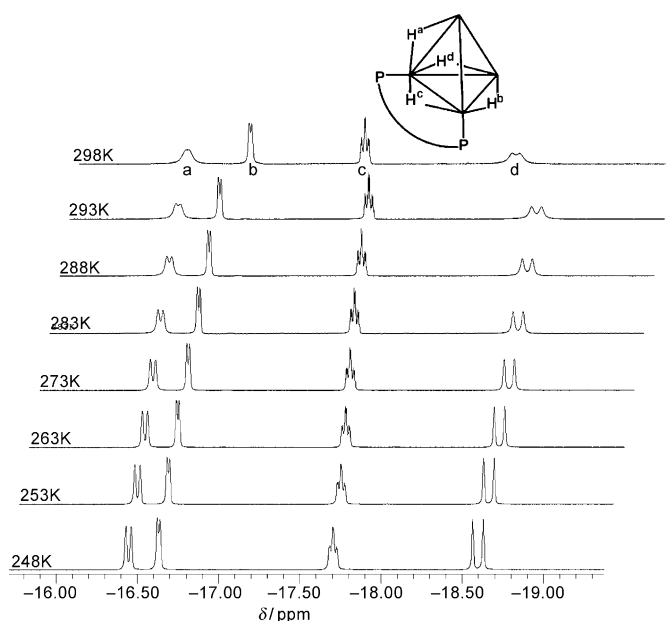


Figure 5. VT NMR spectra of cluster  $[\text{H}_4\text{Ru}_4(\text{CO})_{10}(\mu\text{-1,2-2a})]$  (**12**) recorded in the temperature range 298–248 K (top to bottom).

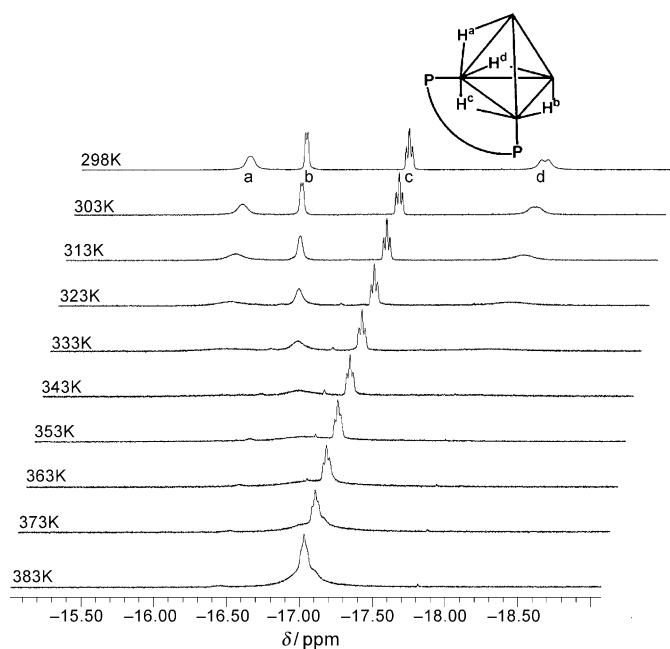


Figure 6. VT NMR spectra of cluster  $[H_4Ru_4(CO)_{10}(\mu-1,2-2a)]$  (**12**) recorded in the temperature range 298–383 K (top to bottom).

phosphorus nuclei in the HetCor spectrum, is the least prone to exchange.

The diphosphine ligand **2b** is structurally very similar to ligand **2a**. It could be coordinated to  $[H_4Ru_4(CO)_{12}]$  most efficiently through thermal substitution, yielding  $[H_4Ru_4(CO)_{10}(\mu-1,2-2b)]$  (**15**) as the sole product in 46% yield. Oxidative decarbonylation gave the two isomers  $[H_4Ru_4(CO)_{10}(1,1-2b)]$  (**14**) and cluster **15**, but in significantly lower yields—**14** (2%) and **15** (22%)—compared with the similar reaction using ligand **2a**. The reaction with

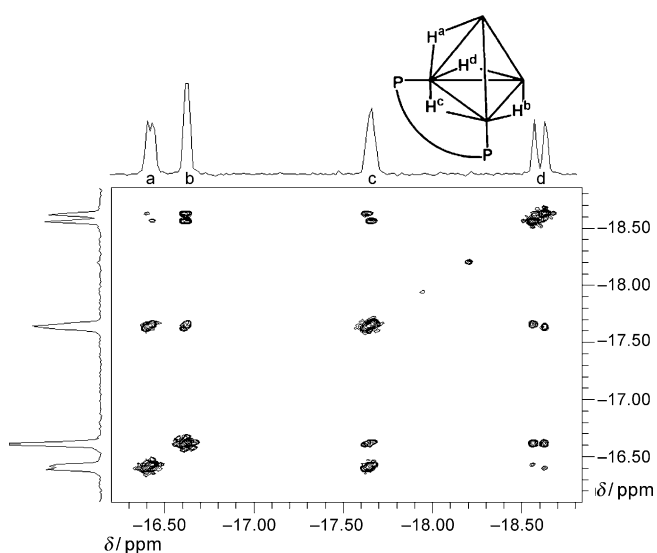


Figure 7. COSY spectrum of cluster  $[H_4Ru_4(CO)_{10}(\mu-1,2-2a)]$  (**12**) recorded at 263 K in  $CD_2Cl_2$ . Note that the peaks at  $\delta = -16.4$  and  $-16.6$  ppm do not have any cross couplings.

ligand **2c** and the parent cluster  $[H_4Ru_4(CO)_{12}]$  by oxidative decarbonylation yields two main products,  $[H_4Ru_4(CO)_{10}(1,1-2c)]$  (**16**) (16%) and  $[H_4Ru_4(CO)_{10}(\mu-1,2-2c)]$  (**17**) (56%). The thermal substitution of  $[H_4Ru_4(CO)_{12}]$  with ligand **2c** led exclusively to cluster  $[H_4Ru_4(CO)_{10}(\mu-1,2-2c)]$  (**17**) in 66% yield. The yield for **16** (16%) in the oxidative

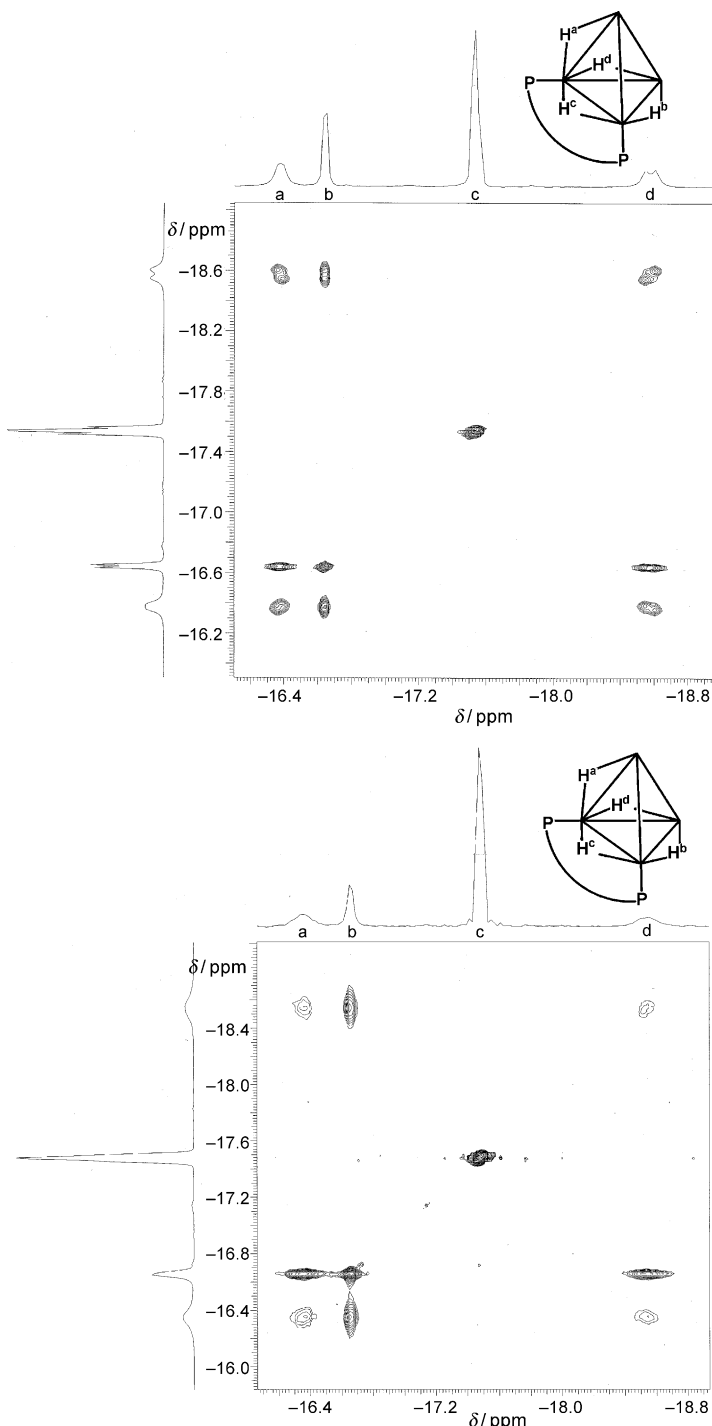


Figure 8. Top: EXSY spectrum of cluster  $[H_4Ru_4(CO)_{10}(\mu-1,2-2a)]$  (**12**) recorded at 298 K with a mixing time of 0.5 s. Bottom: EXSY spectrum of cluster  $[H_4Ru_4(CO)_{10}(\mu-1,2-2a)]$  (**12**) recorded at 313 K with a mixing time of 0.5 s.

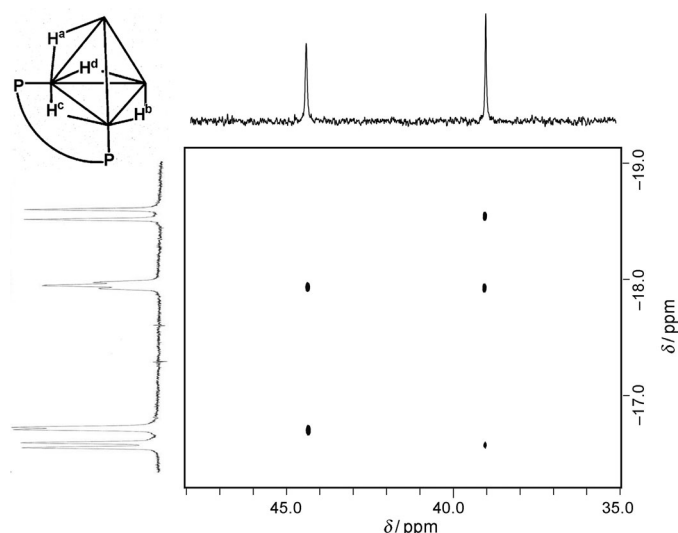


Figure 9.  $^1\text{H},^{31}\text{P}$  HetCor spectrum of cluster  $[\text{H}_4\text{Ru}_4(\text{CO})_{10}(\mu\text{-}1,2\text{-}2\mathbf{a})]$  (**12**) recorded at 223 K in  $[\text{D}_3]\text{chloroform}$  solution. The spectrum reveals the following  $^1\text{H},^{31}\text{P}$  correlation peaks: the hydrides  $\text{H}^b$  and  $\text{H}^d$  correlate with the phosphorus atom at  $\delta = 39.1$  ppm, the hydride  $\text{H}^b$  couples with the phosphorus atom at higher frequency and the hydride  $\text{H}^c$  correlates with both phosphorus nuclei.

decarbonylation reaction is notably higher than those of clusters **11** and **14**. Ligand substitution with **2d** yields one main product,  $[\text{H}_4\text{Ru}_4(\text{CO})_{10}(\mu\text{-}1,2\text{-}2\mathbf{d})]$  (**18**), by both the oxidative decarbonylation and the thermal substitution methods. Similarly, reactions with the diphosphine ligands **2e–2g** yield the clusters  $[\text{H}_4\text{Ru}_4(\text{CO})_{10}(\mu\text{-}1,2\text{-}2\mathbf{e})]$  (**19**),  $[\text{H}_4\text{Ru}_4(\text{CO})_{10}(\mu\text{-}1,2\text{-}2\mathbf{f})]$  (**20**) and  $[\text{H}_4\text{Ru}_4(\text{CO})_{10}(\mu\text{-}1,2\text{-}2\mathbf{g})]$  (**21**). The structures of clusters **15–21** could be identified by comparison of their IR spectra to those of the analogous **2a**-substituted clusters and in the case of clusters **15**, **17**, **19**, **20** and **21** the structures of the clusters were confirmed by X-ray crystallography (see below). See Table 3 for schematic structures for all new clusters isolated in this report.

#### Crystal and molecular structures of clusters **12**, **13**, **15**, **17** and **19–21**

*General description of the molecular structures:* The clusters contain pseudo-tetrahedral  $\text{H}_4\text{Ru}_4$  cores. All four hydrides coordinate to at least one of the ruthenium atoms that are coordinated to the phosphine moieties of the ligand so that the hydride arrangement yields a  $C_s$  symmetry (Figure 10) of the  $\text{H}_4\text{Ru}_4$  cluster core. All carbonyl ligands are bound in

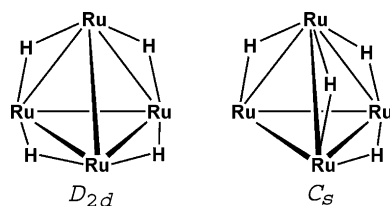


Figure 10. Symmetry of the  $\text{H}_4\text{Ru}_4$  cluster framework.

a terminal monodentate coordination mode. As observed for clusters **4** and **7–9**, the Ru–Ru bond lengths may be separated into two “short” and four “long” metal–metal bonds. In the molecular structures of clusters **12**, **15**, **17** and **19–21**, the ligands were found to exclusively coordinate in a bridging fashion, except for cluster **13** where the diphosphine exhibits a monodentate coordination mode. The  $[\text{H}_4\text{Ru}_4(\text{CO})_{10}(1,2\text{-Walphos})]$  clusters **12**, **15**, **17** and **19–21** exhibit a coordination mode for the diphosphine that is different from their Josiphos counterparts **4** and **8**.

The “bites” of ligands **2a–2g** are so large that it is not possible for the two phosphorus atoms of the ligand to reside in the same relative positions on the same triangular metal face to which both phosphine moieties are coordinated. In the nine-membered “dimetallacycle” that is formed, one phosphorus atom coordinates in an equatorial position, whereas the second phosphorus atom resides in an axial position of the specific triangular face. This coordination mode of a diphosphine ligand on the tetrahedral  $\text{H}_4\text{Ru}_4$  core has not been observed previously, with exception for the dimeric cluster  $[\{\text{H}_4\text{Ru}_4(\text{CO})_{10}(1,2\text{-DIOP})\}_2]$ , in which two diphosphine ligands form bridges between two tetraruthenium units so that each  $\text{H}_4\text{Ru}_4$  unit is coordinated by two phosphorus atoms originating from two different diphosphine ligands.<sup>[21]</sup>

*Molecular structure of  $[\text{H}_4\text{Ru}_4(\text{CO})_{10}(\mu\text{-}1,2\text{-}2\mathbf{a})]$  (**12**):*<sup>[20]</sup> The molecular structure of cluster **12** is shown in Figure 11 and relevant bond lengths and angles are reported in Table 5. The arrangement of the four hydrides yields a  $C_s$  symmetry of the tetrahedral  $\text{H}_4\text{Ru}_4$  cluster core, observed in numerous examples of diphosphine-derivatised ruthenium clusters of the type  $[\text{H}_4\text{Ru}_4(\text{CO})_{10}(\text{diphosphine})]$ <sup>[15,21,24]</sup> The Ru–Ru bond lengths are divided into two distinctive classes—the four hydrido-bridged Ru–Ru bonds are “long” (Ru–

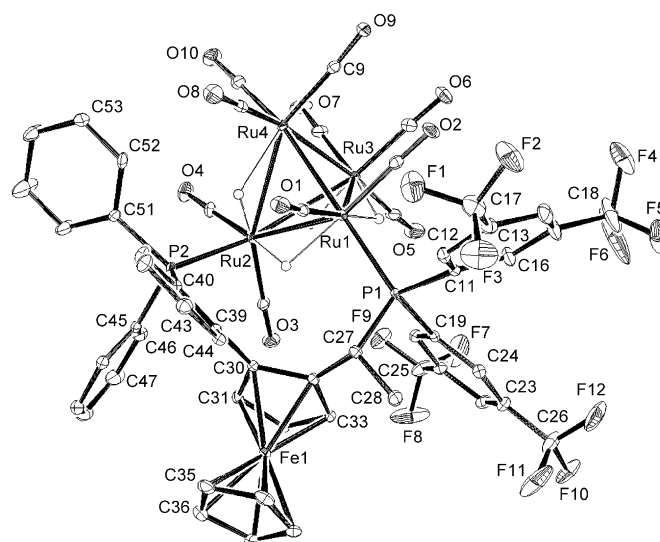


Figure 11. ORTEP drawing of the molecular structure of  $[\text{H}_4\text{Ru}_4(\text{CO})_{10}(\mu\text{-}1,2\text{-}2\mathbf{a})]$  (**12**). Thermal ellipsoids are drawn at the 30% probability level. For the sake of clarity, all hydrogen atoms except the hydrides have been omitted.

Table 5. Selected bond lengths [ $\text{\AA}$ ] and angles [ $^\circ$ ] for clusters **12**, **13**, **15**, **17** and **19–21**.

	<b>12</b>	<b>13</b>	<b>15</b>	<b>17</b>	<b>19</b>	<b>20</b>	<b>21</b>
Ru1–Ru2	3.0277(7) <sup>[a]</sup>	2.9732(5)	3.0032(15) <sup>[a]</sup>	2.9579(6) <sup>[a]</sup>	3.0417(4) <sup>[a]</sup>	3.0215(6) <sup>[a]</sup>	2.9943(5) <sup>[a]</sup>
Ru1–Ru3	2.9224(7) <sup>[a]</sup>	2.9821(5)	2.7774(14)	2.9960(5) <sup>[a]</sup>	2.7790(4)	2.7668(6)	2.9894(6) <sup>[a]</sup>
Ru1–Ru4	2.7635(7)	3.0022(5)	2.9205(13) <sup>[a]</sup>	2.9062(6) <sup>[a]</sup>	2.9111(3) <sup>[a]</sup>	2.9239(7) <sup>[a]</sup>	3.0259(6) <sup>[a]</sup>
Ru2–Ru3	3.0283(6) <sup>[a]</sup>	2.7832(5)	2.9525(15) <sup>[a]</sup>	2.9883(6) <sup>[a]</sup>	2.9986(4) <sup>[a]</sup>	3.0178(7) <sup>[a]</sup>	2.7761(6)
Ru2–Ru4	2.9997(9) <sup>[a]</sup>	2.7854(5)	3.0291(15) <sup>[a]</sup>	2.8936(6)	3.0139(4) <sup>[a]</sup>	2.9938(7) <sup>[a]</sup>	2.9215(6) <sup>[a]</sup>
Ru3–Ru4	2.7785(6)	2.9267(5)	2.7900(15)	2.7722(6)	2.7938(4)	2.7787(7)	2.7846(6)
Ru1–P1	2.3249(10)	2.3765(12)	2.369(3)	2.3641(15)	2.3470(9)	2.3293(15)	2.3663(13)
Ru2–P2	2.3598(10)	2.355(3)	2.355(3)	2.3825(14)	2.3570(9)	2.3898(16)	2.3444(14)
P...P <sup>[b]</sup>	5.584		5.557	5.355	5.544	5.544	5.617
P1–Ru1–Ru2	116.28(3)	162.61(3)	120.73(10)	121.20(4)	117.33(2)	114.80(4)	109.17(3)
P2–Ru2–Ru1	108.23(3)		107.15(9)	119.28(4)	105.57(2)	106.19(4)	116.81(4)
P1–Ru1–Ru2–P2	82.73(3)		74.68(13)	7.89	81.86	85.48	83.03

[a] Ru–Ru bond bridged by hydride. [b] Measured with the Mercury software (<http://www.ccdc.cam.ac.uk/products/mercury/>).

$Ru_{\text{average}} = 2.99 \text{ \AA}$ ) and the two non-bridged Ru–Ru bonds are “short” ( $Ru-Ru_{\text{average}} = 2.77 \text{ \AA}$ ). The average Ru–Ru bond lengths in cluster **12** are comparable with other  $[H_4Ru_4(CO)_{10}(\mu-1,2\text{-diphosphine})]$  structures reported, such as those of  $[H_4Ru_4(CO)_{10}(\mu-1,2\text{-bdpp})]$ <sup>[15]</sup> and  $[H_4Ru_4(CO)_{10}(\mu-1,2\text{-dppe})]$ ,<sup>[24]</sup> where the longest Ru–Ru bond length (2.325  $\text{\AA}$ ) is considerably shorter than the Ru2–P2 bond length (2.360  $\text{\AA}$ ), but not unusual for this type of cluster. Because of the different coordination mode discussed above, the P1–Ru1–Ru2–P2 torsion angle (82.73 $^\circ$ ) is exceptionally large, compared to that observed for clusters **4** (3.05 $^\circ$ ) and **8** (6.02 $^\circ$ ). The P...P separation of 5.584  $\text{\AA}$  in **12** is also exceptionally large when compared to the structures of other  $[H_4Ru_4(CO)_{10}(\mu-1,2\text{-P-P})]$  clusters, for example, in  $[H_4Ru_4(CO)_{10}(\mu-1,2\text{-DIOP})]$ ,<sup>[21]</sup> in which the diphosphine forms an eight-membered “dimetallacycle”, a P...P separation of 4.87  $\text{\AA}$  is found.

**Molecular structure of  $[H_4Ru_4(CO)_{11}(2a)]$  (**13**):** The molecular structure of cluster **13** is shown in Figure 12 and relevant bond lengths and angles are reported in Table 5. To our knowledge, this is the first reported molecular structure with monodentate coordination of a diphosphine to the  $H_4Ru_4$  core. The two short Ru–Ru distances have an average value of 2.784  $\text{\AA}$ , whereas  $Ru-Ru_{\text{average}}$  for the four “long” distances is 2.971  $\text{\AA}$ . The longest Ru–Ru bond is found between Ru1 and Ru4 (3.0022(5)  $\text{\AA}$ ), which is notably shorter than the longest bond in cluster **12**, which is 3.0283(6)  $\text{\AA}$  for the Ru2–Ru3 bond. The Ru1–P1 distance of 2.3765(12)  $\text{\AA}$  is somewhat shorter than that found for the same phosphine moiety in **12** but considerably longer than those found in the related structures of  $[H_4Ru_4(CO)_{11}(PPh_3)]$  (2.354  $\text{\AA}$ ),<sup>[26]</sup>  $[H_4Ru_4(CO)_{11}\{P(Me_2Ph)\}]$  (2.345  $\text{\AA}$ )<sup>[26]</sup> and  $[H_4Ru_4(CO)_{11}\{P(C_6F_5)_3\}]$  (2.362  $\text{\AA}$ ).<sup>[27]</sup>

**Molecular structure of  $[H_4Ru_4(CO)_{10}(\mu-1,2-2b)]$  (**15**):**<sup>[20]</sup> The molecular structure of **15** is shown in Figure 13 and relevant bond lengths and angles are reported in Table 5. The bond lengths in **15** are similar to those observed for related clusters, and the Ru–Ru distances also follow the trend of two

“short” and four “long”, where the four long bonds correspond to those bridged by hydrides. Unlike the related structures  $[H_4Ru_4(CO)_{10}(\mu-1,2\text{-bdpp})]$ <sup>[15]</sup> and  $[H_4Ru_4(CO)_{10}(\mu-1,2\text{-dppe})]$ ,<sup>[24]</sup> where the longest Ru–Ru bond is that bridged by the diphosphine, the longest Ru–Ru distance in cluster **15** is Ru2–Ru4 (3.0291(15)  $\text{\AA}$ ). The Ru1–P1 bond (2.369(3)  $\text{\AA}$ ) is considerably longer compared to the Ru1–P1 bond found in cluster **12** (2.3249(10)  $\text{\AA}$ ). As in

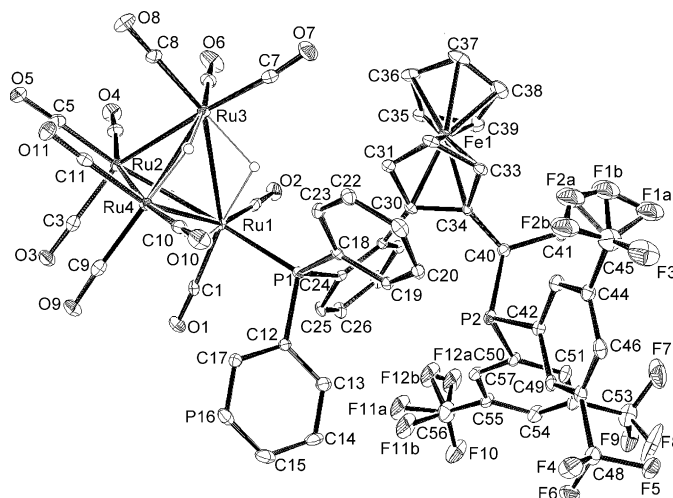


Figure 12. ORTEP drawing of the molecular structure of  $[H_4Ru_4(CO)_{11}\text{-}(2a)]$  (**13**). Thermal ellipsoids are drawn at the 30% probability level. For the sake of clarity, all hydrogen atoms except the hydrides have been omitted.

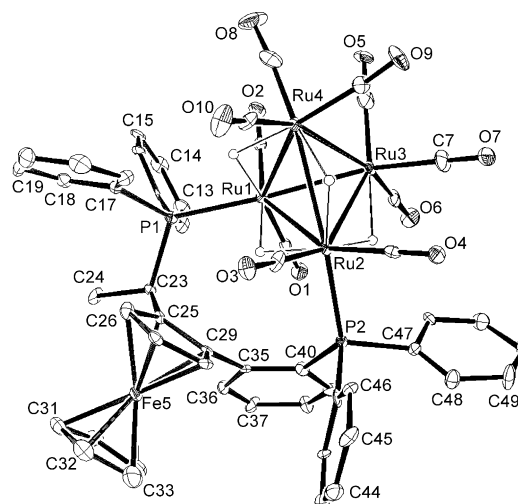


Figure 13. ORTEP drawing of the molecular structure of  $[H_4Ru_4(CO)_{10}(\mu-1,2-2b)]$  (**15**). Thermal ellipsoids are drawn at the 30% probability level. For the sake of clarity, all hydrogen atoms except the hydrides have been omitted.

**12**, the coordinated ligand in cluster **15** yields a nine-membered “dimetallacycle”, where one phosphorus atom is coordinated in an equatorial position and the other phosphorus atom occupies an axial position on the specific triangular face, with a P1–Ru1–Ru2–P2 torsion angle of 74.68°, which is considerably smaller than that found in cluster **12**. The P...P separation found in **15** (5.557 Å), is slightly shorter than the corresponding distance in **12** (5.584 Å).

*Molecular structure of  $[H_4Ru_4(CO)_{10}(\mu-1,2-2c)]$  (**17**):* The molecular structure of **17**, which is shown in Figure 14 (relevant bond lengths and angles are reported in Table 5), has a **2c** ligand coordinated in a bridging mode giving rise to a nine-membered “dimetallacycle”. However, unlike clusters **12** and **15**, the phosphine moieties in **17** are coordinated in the same relative positions to the specific triangular face. The torsion angle P1–Ru1–Ru2–P2 (7.89°) is thus similar to that found in cluster **8** but deviates markedly from those found for clusters **12** and **15**. It seems that the steric bulk of the cyclohexyl substituents on P2 are not sufficiently large (and rigid) to force the phosphorus atoms to occupy equatorial–axial positions. The Ru–P distances of 2.3641(15) (Ru1–P1) and 2.3825(14) Å (Ru2–P2) are slightly longer than those found in **15** but similar to those found in cluster **7**. The P...P distance is 5.355 Å, shorter than those of both **12** (5.584 Å) and **15** (5.557 Å).

*Molecular structure of  $[H_4Ru_4(CO)_{10}(\mu-1,2-2e)]$  (**19**):* The molecular structure of cluster **19** is shown in Figure 15 and relevant bond lengths and angles are summarised in Table 5. The structure of cluster **19** is very similar to those of **12** and **15**. The longest Ru–Ru distance in **19** (3.0417(4) Å) is located between the ruthenium atoms bridged by the diphosphine ligand (Ru1 and Ru2). The torsion angle P1–Ru1–Ru2–P2 measures 81.86°. The P...P separation is 5.54 Å. The Ru2–P2 distance (2.3570(9) Å) is comparable with the

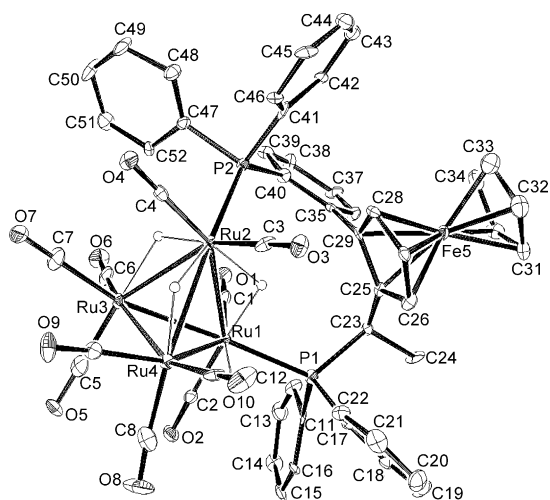


Figure 14. ORTEP drawing of the molecular structure of  $[H_4Ru_4(CO)_{10}(\mu-1,2-2c)]$  (**17**). Thermal ellipsoids are drawn at the 30% probability level. For the sake of clarity, all hydrogen atoms except the hydrides have been omitted.

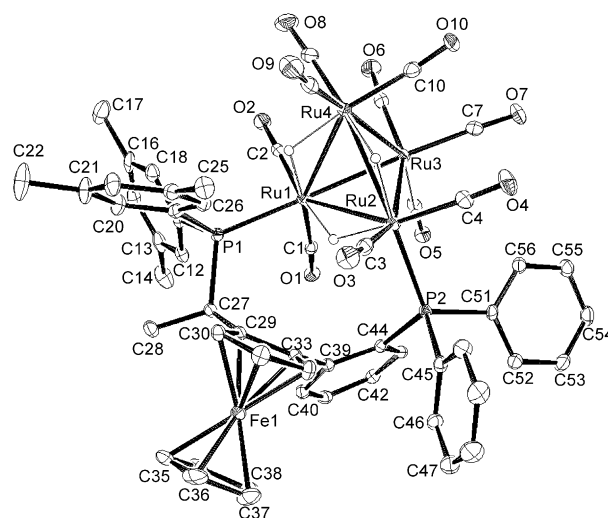


Figure 15. ORTEP drawing of the molecular structure of  $[H_4Ru_4(CO)_{10}(\mu-1,2-2e)]$  (**19**). Thermal ellipsoids are drawn at the 30% probability level. For the sake of clarity, all hydrogen atoms except the hydrides have been omitted.

Ru2–P2 (2.355(3) Å) found in **15**. However, the Ru1–P1 bond length in **19** is shorter than that found in cluster **15**, 2.3470(9) and 2.369(3) Å, respectively.

*Molecular structure of  $[H_4Ru_4(CO)_{10}(\mu-1,2-2f)]$  (**20**):* The molecular structure of cluster **20** is shown in Figure 16 and relevant bond lengths and angles are summarised in Table 5. The structure is similar to those of clusters **12**, **15**, and **19**. As for **19**, but unlike clusters **12**, **15** and **17**, the longest Ru–Ru bond in **20** (3.0215(6) Å) is that bridged by the diphosphine (Ru1–Ru2). The Ru1–P1 distance (2.3293(15) Å) is similar to that found in **12**. The Ru2–P2 bond (2.3898(16) Å) is found to be significantly longer than the Ru1–P1 bond, and is similar to that found in cluster **17**. The two phosphorus atoms in the axial–equatorial position on the specific triangular face are separated by 5.544 Å (within the estimated standard deviations), which is identical to that found in cluster **19**. The torsion angle P1–Ru1–Ru2–P2 measures 85.48°, which is the largest such angle that has been detected in this study.

*Molecular structure of  $[H_4Ru_4(CO)_{10}(\mu-1,2-2g)]$  (**21**):* The molecular structure of cluster **21** is shown in Figure 17 and relevant bond lengths are shown in Table 5. The structure is very similar to those of clusters **12** and **17**. The longest Ru–Ru distance is the Ru1–Ru4 edge (3.0259(6) Å), which is bridged by one hydride. The two phosphorus atoms of the coordinated ligand are separated by 5.62 Å with a torsion angle of 83.03°. This P...P separation is slightly longer than the analogous distance found in **12** (5.58 Å). The Ru–P bonds are slightly asymmetric in lengths (2.3663(13) for Ru1–P1 and 2.3444(14) Å for Ru2–P2), but do not deviate from those observed for other clusters reported here.

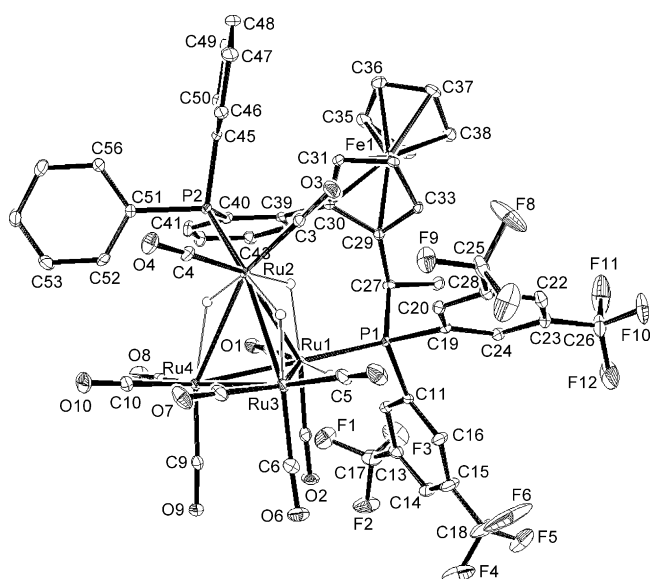


Figure 16. ORTEP drawing of the molecular structure of  $[\text{H}_4\text{Ru}_4(\text{CO})_{10}(\mu\text{-}1,2\text{-}2\text{f})]$  (**20**). Thermal ellipsoids are drawn at the 30% probability level. For the sake of clarity, all hydrogen atoms except the hydrides have been omitted.

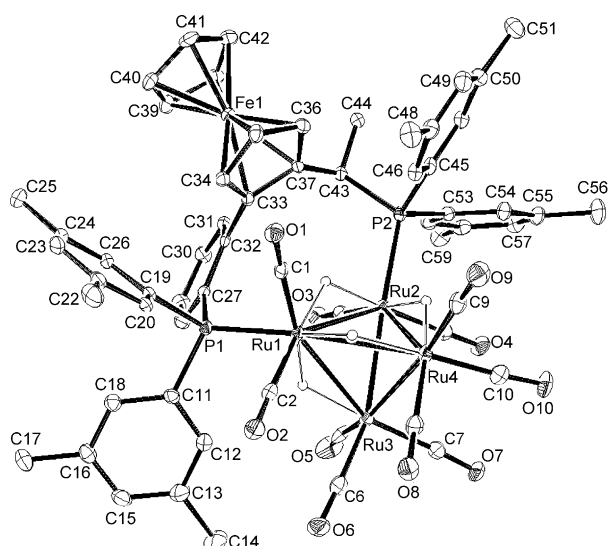


Figure 17. ORTEP drawing of molecular structure of  $[\text{H}_4\text{Ru}_4(\text{CO})_{10}(\mu\text{-}1,2\text{-}2\text{g})]$  (**21**). Thermal ellipsoids are drawn at the 30% probability level. For the sake of clarity, all hydrogen atoms except the hydrides have been omitted.

**Interconversion of isomers:** As mentioned above, the conversion of  $[\text{H}_4\text{Ru}_4(\text{CO})_{10}(\mu\text{-}1,2\text{-}P\text{-}P)]$  clusters into the analogous, thermodynamically favoured,  $[\text{H}_4\text{Ru}_4(\text{CO})_{10}(1,1\text{-}P\text{-}P)]$  isomers has been established for a number of systems.<sup>[15,21,23,24]</sup> For the clusters containing ligand **2a** the opposite isomerisation was detected, that is, in solution  $[\text{H}_4\text{Ru}_4(\text{CO})_{10}(1,1\text{-}2\text{a})]$  (**11**) isomerises into  $[\text{H}_4\text{Ru}_4(\text{CO})_{10}(\mu\text{-}1,2\text{-}2\text{a})]$  (**12**) without any significant cluster fragmentation. Furthermore,  $[\text{H}_4\text{Ru}_4(\text{CO})_{11}(2\text{a})]$  (**13**) loses a CO ligand in

solution to form **12**. Thus, a pure sample of cluster **13** was dissolved in a dichloromethane/hexane mixture and was left to recrystallise at room temperature ( $\approx 21^\circ\text{C}$ ). After approximately two days, red shiny crystals were formed, but their IR spectrum (in dichloromethane) revealed that cluster **12** had been formed. However, the solids of clusters **11** and **13** could be stored at  $+4^\circ\text{C}$  for months without any observed isomerisation.

The rate of the isomerisation of **11** to **12** was affected both by temperature and the polarity of the solvent used. When the ligand substitution reaction was carried out in a mixture of dichloromethane/acetonitrile, cluster **12** was the only isolated product. The isomerisation process of **11** into **12** was followed by  $^1\text{H}$  and  $^{31}\text{P}$  NMR spectroscopy (298 K,  $\text{CDCl}_3$ ) (see Figure 18 and the Supporting Information) during a period of 30 days. A sample of **11** (10 mg,  $6.17\ \mu\text{mol}$ ) in  $\text{CD}_3\text{Cl}$  (0.5 mL) was prepared in a 5 mm standard NMR tube. The sample was stored at room temperature ( $\approx 21^\circ\text{C}$ ) when not being analysed. The proton spectra (hydride resonances only) (Figure 18) show the transformation of **11** into **12**, which proceeded at a relatively slow rate. The top spectrum in Figure 18 displays the hydrides of the freshly made sample of **11**, which exhibits relatively sharp resonances at  $\delta = -15.67(\text{s})$ ,  $-15.97(\text{s})$ ,  $-16.51(\text{brm})$  and  $-16.75\ \text{ppm}(\text{s})$ . After two days ( $t=2$ ), a new set of four new hydride resonances that could be assigned to **12** was observed at  $\delta = -16.4$ ,  $-16.7$ ,  $-17.6$  and  $-18.5\ \text{ppm}$ . In addition to the appearance of the four hydrides of cluster **12**,

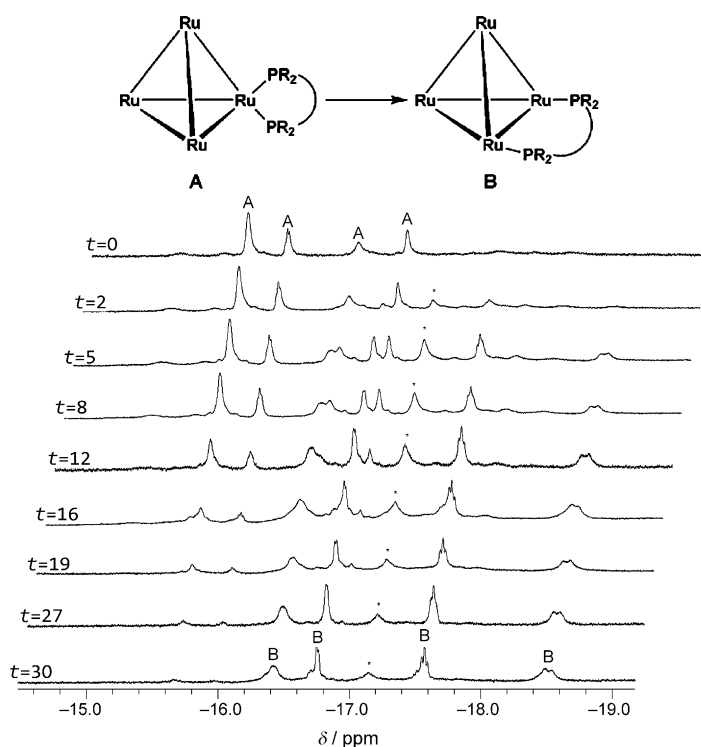


Figure 18. Arrayed  $^1\text{H}$  NMR spectra illustrating the isomerisation process of  $[\text{H}_4\text{Ru}_4(\text{CO})_{10}(1,1\text{-}2\text{a})]$  (**11**) into  $[\text{H}_4\text{Ru}_4(\text{CO})_{10}(\mu\text{-}1,2\text{-}2\text{a})]$  (**12**) recorded in  $\text{CDCl}_3$  at 298 K ( $t$  = number of days). The broad signal at  $\delta = -17.15\ \text{ppm}$  labelled \* is from the four fluxional hydrides of cluster  $[\text{H}_4\text{Ru}_4(\text{CO})_{11}(2\text{a})]$  (**13**).

a broad signal at  $\delta = -17.15$  ppm became notably strong ( $t = 5$ ), which may be assigned to the hydride resonances for cluster **13** (see the Experimental Section). As the isomerisation proceeds, the resonances from cluster **11** are completely gone after approximately 30 days. At the end of the experiment, there was still a small amount of **13** present in the solution. The complementary  $^{31}\text{P}$  NMR spectra confirm the  $^1\text{H}$  NMR analyses, that is, transformation of **11** into **12**, with concomitant formation and disappearance of **13**, but do also reveal the appearance of free diphosphine ligand and the corresponding phosphine oxide during the prolonged reaction time. It appears that decomposition of the cluster occurs on prolonged standing in solution (30 days), but that the main species formed is the thermodynamically stable isomer **12** in which the diphosphine bridges a Ru–Ru bond.

Like cluster **11**,  $[\text{H}_4\text{Ru}_4(\text{CO})_{10}(1,1\text{-}2\text{c})]$  (**16**) shows similar reluctance to retain the chelating coordination mode. Even though this cluster (**16**) could be synthesised in considerably higher yield than its analogues **11** and **14**, it is also unstable in solution. Once **16** is exposed to polar solvents (such as dichloromethane or chloroform), isomerisation occurs at a high rate. TLC, IR and NMR analyses reveal that within minutes a significant amount of cluster  $[\text{H}_4\text{Ru}_4(\text{CO})_{10}(\mu\text{-}1,2\text{-}2\text{c})]$  (**17**) has been formed. It is likely that the eight-membered metallacycle that is formed when a Walphos ligand coordinates in a chelating mode is more strained than the nine-membered “dimetallacycle” that is formed in the bridging mode, and that it is the relief of this strain that is the driving force for the isomerisation reaction.

**Electrochemistry:** The ferrocene-based diphosphine ligands used in this study are not expected to display straightforward electrochemistry, as the oxidised species will have considerable P-centred radical character that can give rise to complex reactions on the cyclic voltammetric timescale, including decomposition.<sup>[28]</sup> In order to establish whether the redox properties of these ligands are affected by their coordination to metals, and whether the metal clusters themselves could be reversibly reduced and/or oxidised, a preliminary electrochemical study of the ferrocenyl-based diphosphine ligand **2a** and its tetranuclear hydridoruthenium carbonyl cluster complex **12** was undertaken by using cyclic voltammetry at a platinum disk electrode. Experiments were performed on acetonitrile solutions containing 0.1 M tetra-*n*-butylammonium perchlorate as background electrolyte, by using a standard three-electrode system. The results are summarised in Table 6.

For ligand **2a** no reductive electrochemistry was detected down to the solvent/electrolyte limit of approximately  $-2.2$  V. However, the anodic electrochemistry (see Figure 19) displays the expected oxidation of the ligand ferrocenyl group at exactly the same potential as recorded for the reference ferrocene under the same conditions ( $E_{\text{pa}} = +0.15$  V vs.  $\text{Ag}/\text{Ag}^+$ , see the Experimental Section), but with no corresponding reduction peak, even when the scan rate was increased in steps from the normally used 100 up to  $2000$   $\text{mV s}^{-1}$ . In addition, reversing the anodic scan at

Table 6. Redox potentials (V vs.  $\text{Ag}/\text{Ag}^+$ ) of the ferrocene reference, the Walphos ligand **2a** and  $[\text{H}_4\text{Ru}_4(\text{CO})_{10}(\mu\text{-}1,2\text{-}2\text{a})]$  (**12**).<sup>[a]</sup>

Compound	Oxidation processes		Reduction processes	
	$E_{\text{pa}}$	$E_{\text{pc}}$	$E_{\text{pc}}$	$E_{\text{pa}}$
ferrocene	+0.15	+0.03		
<b>2a</b>	+0.15	–		
	+0.36 <sup>[b]</sup>	+0.28 <sup>[b]</sup>		
	+0.45	+0.37 <sup>[b]</sup>		
	+0.66	+0.59 <sup>[b]</sup>		
	+0.27 <sup>[c]</sup>	+0.21 <sup>[b,c]</sup>	–1.55	–
<b>12</b>	+0.40	–	–1.92	–
			–	–1.01

[a] Measured in  $\text{CH}_3\text{CN}$  containing 0.1 M  $[n\text{Bu}_4\text{N}][\text{ClO}_4]$  at a scan rate of  $100$   $\text{mV s}^{-1}$  (unless otherwise indicated) and referenced to  $\text{Ag}/\text{Ag}^+$  (see body of table and the Experimental Section for corresponding ferrocene/ferrocenium values).  $E_{\text{pa}}$  = anodic peak potential,  $E_{\text{pc}}$  = cathodic peak potential. [b] Estimated value: peak poorly defined. [c] Scan rate =  $1000$   $\text{mV s}^{-1}$ .

+0.28 V (before reaching the potentials of the other oxidative processes mentioned below) resulted in the same irreversible profile, showing that the ferrocenyl cation generated must immediately react to form some non-reducible product without the participation of the species generated at more anodic potential. Here three further oxidation waves were observed (one barely detected, see Figure 19;  $E_{\text{p}}$  values in Table 6), each with an associated but poorly resolved reductive counterpart observed upon reversing the scan; varying the scan rate in steps between 20 and  $2000$   $\text{mV s}^{-1}$  did not enhance the definition of these peaks. The processes involved at these more positive potentials are likely to involve oxidation of the two differently substituted phosphine groups in the ligand, but further interpretation is not feasible.

A somewhat more complicated voltammetric behaviour is exhibited by the tetranuclear complex **12**, although the

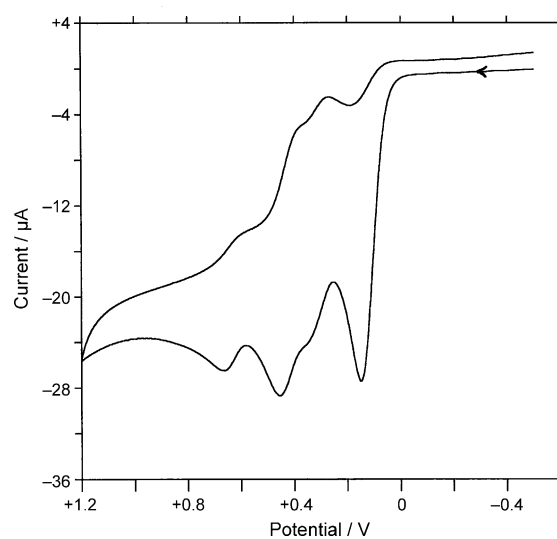


Figure 19. Cyclic voltammogram (oxidation processes) of ligand **2a** in  $\text{CH}_3\text{CN}$  at a scan rate of  $100$   $\text{mV s}^{-1}$ . The potential scale is referenced to  $\text{Ag}/\text{Ag}^+$  (see the Experimental Section). The scan started at  $-0.50$  V.

general features observed by Hartl, Johnson and co-workers<sup>[29]</sup> in their detailed study of the  $\alpha$ -diimine complexes of the tetranuclear hydridoruthenium carbonyl clusters  $[\text{H}_4\text{Ru}_4(\text{CO})_{10}(\text{L})]$  ( $\text{L} = 2,2'$ -bipyrimidine, 2,3-bis(pyridin-2-yl)pyrazine or 2,2'-bipyridine) in tetrahydrofuran solution are retained. Thus, in reductive scans we observe two cathodic peaks at rather negative potential (see Figure 20) that,

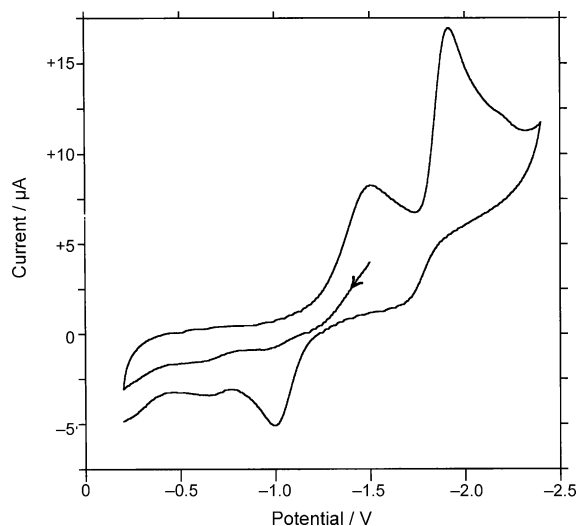


Figure 20. Cyclic voltammogram (reduction processes) of  $[\text{H}_4\text{Ru}_4(\text{CO})_{10}(\mu\text{-}1,2\text{-}2\mathbf{a})]$  ( $\mathbf{12}$ ) in  $\text{CH}_3\text{CN}$  at a scan rate of  $100 \text{ mV s}^{-1}$ . The potential scale is referenced to  $\text{Ag}/\text{Ag}^+$  (see the Experimental Section). The scan started at  $-1.50 \text{ V}$  and shows that the anodic peak at  $-1.01 \text{ V}$  is only obtained after the reductive scan.

by analogy with the corresponding  $\alpha$ -diimine complexes,<sup>[29]</sup> can be ascribed to a one-electron process, which produces the radical anion  $\mathbf{12}^{\cdot-}$  ( $E_{\text{pc}} = -1.55 \text{ V}$ , irreversible) and a second one-electron reduction to provide the unstable dianion  $\mathbf{12}^{2-}$  ( $E_{\text{pc}} = -1.92 \text{ V}$ , irreversible), which eliminates dihydrogen to form the dihydrido dianion  $[\text{H}_2\text{Ru}_4(\text{CO})_{10}(1,2\text{-}\mu\text{-}2\mathbf{a})]^{2-}$ . It is the oxidation of this dihydrido dianion that is responsible for the anodic peak observed on the return scan at  $E_{\text{pa}} = -1.01 \text{ V}$ , a peak not observed unless the cathodic peaks referred to above are first traversed (see Figure 20). In contradistinction to the initial reduction of  $[\text{H}_4\text{Ru}_4(\text{CO})_{10}(\alpha\text{-diimine})]$  (in tetrahydrofuran) to produce the radical anion, which was reported<sup>[29]</sup> to be electrochemically and chemically reversible, we find the initial reduction of the diphosphine complex  $\mathbf{12}$  (in acetonitrile) to be irreversible. This was shown by reversing the direction of the reductive scan before onset of the second reduction that forms the unstable dianion: no oxidative wave was observed over a wide range of scan rates. The oxidative electrochemistry of complex  $\mathbf{12}$  displays, at a scan rate of  $100 \text{ mV s}^{-1}$ , a single irreversible anodic peak centred at  $+0.40 \text{ V}$ . Similar behaviour was observed in the oxidative behaviour of  $[\text{H}_4\text{Ru}_4(\text{CO})_{10}(\alpha\text{-diimine})]$ ,<sup>[29]</sup> and this peak can be ascribed to an anodic process localised on the metal core, which may indeed induce cleavage of Ru–Ru bonds. There is no evi-

dence of oxidation of the phosphine groups, in contrast to the observations made in the study of the free diphosphine ligand  $\mathbf{2a}$  (see above); clearly coordination of the phosphorus atoms to the tetraruthenium cluster inhibits such oxidation. However, on increasing the scan rate up to  $1000 \text{ mV s}^{-1}$ , a shoulder on the main anodic peak (which itself shifts slightly to  $+0.46 \text{ V}$ ) becomes resolved at  $+0.27 \text{ V}$  (see Figure 21).

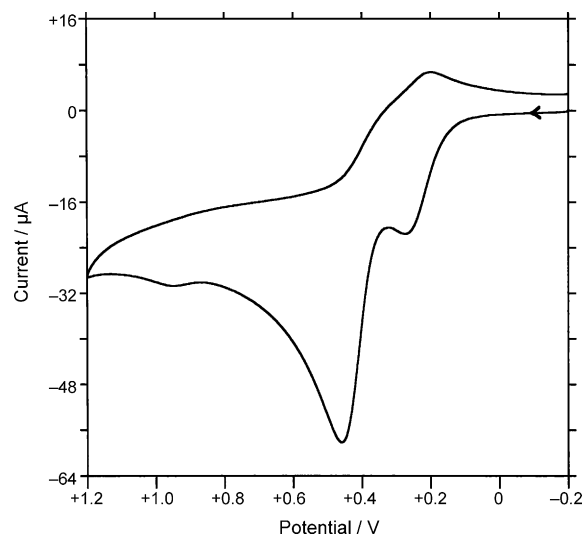
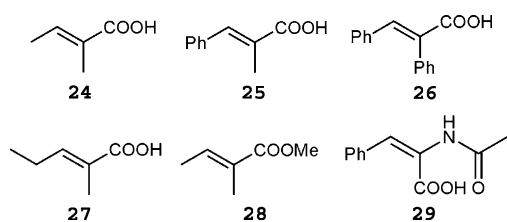


Figure 21. Cyclic voltammogram (oxidation processes) of  $[\text{H}_4\text{Ru}_4(\text{CO})_{10}(\mu\text{-}1,2\text{-}2\mathbf{a})]$  ( $\mathbf{12}$ ) in  $\text{CH}_3\text{CN}$  at a scan rate of  $1000 \text{ mV s}^{-1}$ . The potential scale is referenced to  $\text{Ag}/\text{Ag}^+$  (see the Experimental Section). The scan started at  $-0.20 \text{ V}$ .

This can confidently be ascribed to the oxidation of the ferrocenyl group in the diphosphine ligand, made slightly more anodic than in the free ligand (by  $0.12 \text{ V}$ ) upon coordination of the phosphorus atoms to the tetraruthenium cluster. There is evidence for a corresponding cathodic peak at  $+0.21 \text{ V}$  on the return scan, but this is poorly defined and not improved by reversing the direction of the potential scan before the onset of the main oxidation peak.

**Catalytic activity—asymmetric hydrogenation of  $\alpha$ -unsaturated carboxylic acids:** As mentioned in the introduction, it is well established that chiral diphosphine ligands play an important role in asymmetric hydrogenation.<sup>[3a,30]</sup> In order to assess the capabilities of the new clusters prepared in this investigation to function as catalysts for asymmetric hydrogenation, hydrogenation of the carboxylic acids  $\mathbf{24}$ – $\mathbf{29}$  (Scheme 1) in the presence of clusters  $\mathbf{4}$ ,  $\mathbf{6}$ ,  $\mathbf{8}$ ,  $\mathbf{10}$ – $\mathbf{12}$ ,  $\mathbf{14}$ ,  $\mathbf{15}$  and  $\mathbf{17}$ – $\mathbf{21}$  was examined. In the present study, a hydrogen pressure of  $50 \text{ bar}$  was used, instead of  $130 \text{ bar}$  commonly used in previous cluster-based catalysis tests.<sup>[14b]</sup> The lower hydrogen pressure was expected to enhance the chiral induction, as demonstrated by us in a previous study.<sup>[15]</sup> The results from the catalytic investigation of clusters  $\mathbf{4}$ ,  $\mathbf{6}$ ,  $\mathbf{8}$ ,  $\mathbf{10}$ – $\mathbf{12}$ ,  $\mathbf{14}$ ,  $\mathbf{15}$  and  $\mathbf{17}$ – $\mathbf{21}$  are summarised in Table 7. The clusters that have been investigated in this report are superior to



Scheme 1. Drawings of the substrates used in catalytic experiments. (*E*)-2-methyl-2-butenoic acid (tiglic acid, **24**), (*E*)- $\alpha$ -methyl-cinnamic acid (**25**), (*E*)- $\alpha$ -phenyl-cinnamic acid (**26**), (*E*)-2-methyl-2-pentenoic acid (**27**), (*E*)-methyl 2-methylbut-2-enoate (**28**) and (*E*)- $\alpha$ -acetamidocinnamic acid (**29**).

any previously tested tetrahydrido tetraruthenium cluster<sup>[14,15,21]</sup> as catalysts/catalyst precursors for asymmetric hydrogenation. Clusters **4**, **6**, **8**, **10–12**, **14**, **15** and **17–21** were able to efficiently convert tiglic acid (**24**) (see Table 7) into 2-methylbutanoic acid within 24 h in good yields and in relatively low molar ratios ( $n_{\text{catalyst}}/n_{\text{substrate}} = 1:500$ ).

Although all catalysts were similar in conversion rates of the substrate, the catalysts based on Josiphos derivatives (**1a–1d**) of  $[\text{H}_4\text{Ru}_4(\text{CO})_{12}]$  gave no, or very low, enantioselectivity, whereas the clusters derivatised with the Walphos ligands **2a–2g** resulted in good enantioselectivities. Although catalysts **12**, **15** and **17–21** were recovered in good yields ( $\approx 70\%$ ) after a complete catalytic experiment, only trace amounts (at best) of catalysts **4** and **7–9** could be recovered. Catalyst recycling was investigated by recovering cluster **18** from the hydrogenation of tiglic acid (**24**, Scheme 1) and reusing it in the exact same experiment (corresponding to entry 10, Table 7). Identical conversion rates were observed for the two catalytic runs; the enantioselectivities were not investigated in these specific catalysis experiments.

In the cluster-based hydrogenation effected by  $[\text{H}_4\text{Ru}_4(\text{CO})_{10}\{\mu\text{-}1,2\text{-}(R,R \text{ or } S,S)\text{-bdpp}\}]$ ,<sup>[15]</sup> it was found that these clusters were converted to the structural isomers  $[\text{H}_4\text{Ru}_4(\text{CO})_{10}\{1,1\text{-}(R,R \text{ or } S,S)\text{-bdpp}\}]$  (chelating diphosphine) during the catalytic reactions. In agreement with the opposite trend for the isomerisation reactions mentioned above, this interconversion was observed during the catalytic experiments with clusters **11** and **14**, that is, the “chelating” isomers **11** and **14** were converted to the analogous “bridging” isomers **12** and **15**. No remnants of **11** or **14** could be detected after the catalytic reactions but when cluster **11** was used as a starting material, a second cluster—identified as  $[\text{H}_4\text{Ru}_4(\text{CO})_8(\mathbf{2a})_2]$  on the basis of its mass spectrum—could be detected in addition to the isomer **12**. It thus appears unlikely that **11** and **14** are active catalysts for the hydrogenation reactions.

The catalytic activities of clusters **11**, **12**, **15** and **17–21** were further examined in the asymmetric hydrogenations of (*E*)- $\alpha$ -methyl-cinnamic acid (**25**), (*E*)- $\alpha$ -phenyl-cinnamic acid (**26**) and (*E*)-2-methyl-2-pentenoic acid (**27**) (Scheme 1). The substrates were selected so that a varying degree of bulkiness was achieved.

It has been demonstrated that the carboxylate functionality plays an important role in the interaction between the substrate and the catalyst in hydrogenation reactions utilising mono- and polynuclear ruthenium catalysts.<sup>[14a,31]</sup> For example, Benedetti et al.<sup>[14a]</sup> observed a significant difference in optical purity when comparing the two substrates (*E*)- $\alpha$ -methyl-cinnamic acid (**25**) and ethyl (*E*)- $\alpha$ -methyl-cinnamate when they used the cluster  $[\text{H}_4\text{Ru}_4(\text{CO})_8\{(-)\text{-DIOP}\}_2]$  as catalyst. The hydrogenated cinnamic ester obtained was of considerably lower optical purity than that of the hydrogenated cinnamic acid.

In order to investigate whether the reactivity and the enantioselectivity in the hydrogenation reactions effected by the cluster catalysts/catalyst precursors in this study are dependent on substrates having a carboxylate functionality, a control experiment by using the substrate methyl 2-methylbut-2-enoate (**28**, Scheme 1), that is, the methyl ester of tiglic acid, was performed. The cluster  $[\text{H}_4\text{Ru}_4(\text{CO})_{10}(\mu\text{-}1,2\text{-}\mathbf{2a})]$  (**12**) was used as catalyst with a catalyst/substrate ratio of 1:500. Under standard reaction conditions for catalytic experiments (see the Experimental Section), the results from this experiment revealed a rather low conversion of the substrate (68%). The enantiomeric excess was determined to be 29%, which is a significant decrease in enantioselectivity compared with that obtained when the corresponding carboxylic acid (tiglic acid (**24**), 82% *ee*) was used as substrate under the same reaction conditions (see Table 7). A possible explanation for this result is that the carboxylate functionality is an important factor when the substrate coordinates to the metal centre. A study by Ashby and Halpern<sup>[31]</sup> proposes that tiglic acid in the presence of the mononuclear catalyst  $[\text{Ru}^{\text{II}}(\text{BINAP})(\text{OAc})_2]$  (**22**) coordinates exclusively through the carboxylate group to the ruthenium as the initial step in the catalytic cycle of a hydrogenation. It is thus possible that the initial coordination of the type of substrate used in this study to a potential cluster catalyst occurs through coordination of the carboxylate moiety (see below).

It is known that mononuclear ruthenium complexes are viable as catalysts in the asymmetric hydrogenation of various types of enamides.<sup>[32]</sup> In an attempt to hydrogenate (*E*)- $\alpha$ -acetamidocinnamic acid (**29**) a catalytic test was performed by using cluster **12**. After a period of 24 h the reaction mixture was analysed but it was not possible to detect any hydrogenated product by <sup>1</sup>H NMR spectroscopic analysis.

**Nature of the active catalyst:** Clusters have been used in numerous homogeneous catalysis systems.<sup>[5]</sup> A recent example of enantioselective hydrogenation catalysis involving transition-metal carbonyl clusters is the asymmetric transfer hydrogenation of ketones, where Ikariya and co-workers<sup>[33]</sup> obtained evidence from spectroscopic and reactivity studies that implicate an active catalyst consisting of a trinuclear ruthenium cluster with a chiral diiminodiphosphine ligand. Despite the prevalence of transition-metal carbonyl clusters in homogeneous catalysis, there are no unambiguous proofs

Table 7. Summary of the catalytic asymmetric hydrogenation experiments performed in the presence of clusters **4**, **6**, **8**, **10–12**, **14**, **15** and **17–21** as catalysts.

Entry	Substrate	Catalyst	Solvent	Conversion <sup>[a]</sup> [%]	Selectivity <sup>[b]</sup> [%]	ee [%]	Configuration <sup>[c]</sup>
1	<b>24</b>	<b>4</b>	EtOH/Tol <sup>[d]</sup>	100	97	2:9	S
2	<b>24</b>	<b>6</b>	EtOH/Tol	100	86	8:12	S
3	<b>24</b>	<b>8</b>	EtOH/Tol	100	90	no ee	–
4	<b>24</b>	<b>10</b>	EtOH/Tol	100	96	no ee	–
5	<b>24</b>	<b>11</b>	EtOH/Tol	100	100	92	S
6	<b>24</b>	<b>12</b>	EtOH/Tol	99	99	82	S
7	<b>24</b>	<b>14</b>	EtOH/Tol	100	100	63	S
8	<b>24</b>	<b>15</b>	EtOH/Tol	100	100	58	S
9	<b>24</b>	<b>17</b>	EtOH/Tol	99	100	54	R
10	<b>24</b>	<b>18</b>	EtOH/Tol	87	100	77	S
11	<b>24</b>	<b>19</b>	EtOH/Tol	100	99	62	S
12	<b>24</b>	<b>20</b>	EtOH/Tol	100	100	77	S
13	<b>24</b>	<b>21</b>	EtOH/Tol	100	100	50	S
14	<b>25</b>	<b>11</b>	EtOH/Tol	100	64	89	S
15	<b>25</b>	<b>12</b>	EtOH/Tol	100	91	75	S
16	<b>25</b>	<b>15</b>	EtOH/Tol	100	89	69	S
17	<b>25</b>	<b>17</b>	EtOH/Tol	100	82	44	R
18	<b>25</b>	<b>18</b>	EtOH/Tol	99	91	79	S
19	<b>25</b>	<b>19</b>	EtOH/Tol	100	86	65	S
20	<b>25</b>	<b>20</b>	EtOH/Tol	100	70	71	S
21	<b>25</b>	<b>21</b>	EtOH/Tol	100	93	43	S
22	<b>26</b>	<b>11</b>	EtOH/Tol	100	65	83	R
23	<b>26</b>	<b>12</b>	EtOH/Tol	100	90	66	R
24	<b>26</b>	<b>15</b>	EtOH/Tol	100	83	63	R
25	<b>26</b>	<b>17</b>	EtOH/Tol	90	90	57	S
26	<b>26</b>	<b>18</b>	EtOH/Tol	48	89	60	R
27	<b>26</b>	<b>19</b>	EtOH/Tol	100	90	59	R
28	<b>26</b>	<b>20</b>	EtOH/Tol	100	90	72	R
29	<b>26</b>	<b>21</b>	EtOH/Tol	100	77	38	R
30	<b>27</b>	<b>11</b>	EtOH/Tol	100	100	68	S
31	<b>27</b>	<b>12</b>	EtOH/Tol	100	99	68	S
32	<b>27</b>	<b>15</b>	EtOH/Tol	100	99	42	S
33	<b>27</b>	<b>17</b>	EtOH/Tol	94	81	69	R
34	<b>27</b>	<b>18</b>	EtOH/Tol	100	99	62	S
35	<b>27</b>	<b>19</b>	EtOH/Tol	100	100	43	S
36	<b>27</b>	<b>20</b>	EtOH/Tol	70	99	36	S
37	<b>27</b>	<b>21</b>	EtOH/Tol	100	100	24	S
38	<b>24</b> +Hg <sup>[e]</sup>	<b>12</b>	EtOH/Tol	100	100	87	S
39	<b>24</b> +Hg <sup>[e]</sup>	<b>15</b>	EtOH/Tol	100	100	62	S
40	<b>24</b>	<b>12</b>	acetonitrile	97	100 <sup>[f]</sup>	80	S
41	<b>25</b>	<b>12</b>	acetonitrile	100	100 <sup>[f]</sup>	79	S
42	<b>26</b>	<b>12</b>	acetonitrile	99	100 <sup>[f]</sup>	73	R
43	<b>27</b>	<b>12</b>	acetonitrile	98	100 <sup>[f]</sup>	60	S
44	<b>24</b>	<b>12</b>	benzene	99	100	67	S
45	<b>25</b>	<b>12</b>	benzene	59	100	75	S
46	<b>26</b>	<b>12</b>	benzene	84	100	47	R
47	<b>27</b>	<b>12</b>	benzene	58	100	33	S
48	<b>24</b>	<b>22</b>	EtOH/Tol	100	85	68	S
49	<b>24</b>	<b>23</b>	EtOH/Tol	100	79	30	S

[a] The amount of substrate consumed in the catalytic experiment, assessed by <sup>1</sup>H NMR spectroscopy. [b] The carboxylate of the substrate was found to react with the solvent (ethanol) to form an ester. [c] Favoured enantiomer. [d] Tol = toluene. [e] Mercury poison test. [f] [EtNH<sub>2</sub>] was observed as byproduct.

of clusters being active catalysts. Besides in situ detection of an active cluster catalyst, the only proof that can be obtained is probably the opportunity that the enantioselective catalysis is effected by clusters where the chirality resides in the cluster framework rather than in a ligand.<sup>[34]</sup> It is possible that the active catalysts in cluster-based catalysis are colloids or mononuclear species that are formed in situ. For example, in a recent study, Süss-Fink and co-workers<sup>[35]</sup>

showed that the cluster cation [Ru<sub>3</sub>(μ-H)<sub>3</sub>(η<sup>6</sup>-C<sub>6</sub>H<sub>6</sub>)(η<sup>6</sup>-C<sub>6</sub>Me<sub>6</sub>)<sub>2</sub>(μ<sub>3</sub>-O)]<sup>+</sup>, believed to be an active catalyst for benzene hydrogenation, was actually the source of colloidal Ru<sup>0</sup> particles that were the origin of the catalytic effect. In order to probe the nature of the active catalyst in the hydrogenations effected by [H<sub>4</sub>Ru<sub>4</sub>(CO)<sub>10</sub>(μ-1,2-**2a**) (**12**) and [H<sub>4</sub>Ru<sub>4</sub>(CO)<sub>10</sub>(μ-1,2-**2b**) (**15**), which gave good enantioselectivity, a number of control experiments was carried out.

#### Hydrogenation in the presence of a chiral diphosphine ligand:

A control experiment was conducted to determine whether the ligand **2a** possesses any catalytic activity in the absence of ruthenium metal. In a small autoclave, ligand **2a** and the substrate tiglic acid (**24**) were added in a molar ratio of 1:250. After being heated at 100 °C under 50 bar of H<sub>2</sub> for 72 h, it was found that 23 % of **24** was converted to 2-methylbutanoic acid with an enantiomeric excess of 68 % (S). This remarkable result indicates that **2a** gives strong chiral induction and is capable of acting as a catalyst/catalyst precursor itself, albeit with considerably lower enantioselectivity than the corresponding ruthenium cluster **12**. It is possible that the ligand may be responsible for “background” activity during the cluster-catalysed hydrogenation. However, the rate by which the free ligand **2a** hydrogenates **24** is apparently very low, as indicated by the low conversion rate, and its contribution to the catalytic hydrogenation by using cluster **12** as catalyst must be regarded as limited.

#### Hydrogenation in the absence of a catalyst/catalyst precursor:

To rule out that no metallic residues/contaminations are responsible for the above-mentioned observation and as background activity in other experiments, a similar control experiment was carried out by using standard reaction conditions for the catalytic hydrogenation. In this experiment,

substrate **24** was dissolved in ethanol/toluene (1:1 v/v) in the absence of any potential catalyst, and heated under pressures of H<sub>2</sub>. After 24 h of heating no hydrogenation products were detected. This observation clearly indicates that the temperature and hydrogen pressure used in our catalytic experiments are not forcing enough to cause hydrogenation of **24** and that no apparent metallic contamination that may cause hydrogenation is present.

**Mercury poisoning test:** It is known that forcing conditions, such as high temperatures and high pressures of hydrogen gas, increase the probability that a colloidal catalyst will form. An illustrative example is the well-known Wilkinson catalyst, [Rh<sup>I</sup>Cl(PPh<sub>3</sub>)<sub>3</sub>], which serves as an excellent homogeneous hydrogenation catalyst at ambient temperatures and hydrogen pressures, but generates a colloidal catalyst species when heated at 130 °C under elevated pressure of H<sub>2</sub> (50 psi ≈ 3.4 bar).<sup>[36]</sup> Another example is the Heck reaction, where the palladium catalyst is readily reduced to Pd<sup>0</sup> irrespective of the nature of its catalyst precursor, at temperatures of 120 °C or higher, leading to the formation of soluble Pd colloids that mediate the Heck reaction.<sup>[37]</sup> In order to assess whether colloidal material is formed during the reactions and may be responsible for the catalytic effects observed for the ruthenium clusters in this study, a mercury poisoning test<sup>[38]</sup> was performed. Approximately 2000-fold excess of metallic mercury was added to the hydrogenation of tiglic acid (**24**) by using clusters **12** and **15**. The product analysis revealed that upon addition of Hg<sup>0</sup>, slightly better results were obtained than in the reactions without Hg<sup>0</sup> added. Not only were the selectivities improved but the enantiomeric excess was increased by four to five percentage units (see Table 7, entry 6 vs. entry 38, and entry 8 vs. entry 39). These observations suggest that the cluster does undergo fragmentation and that formation of colloidal materials occurs during the course of reaction. However, the effect of the colloidal material seems very limited for the hydrogenation reaction in general.

**Hydrogenation by chiral mononuclear ruthenium complexes:** It is reasonable to assume that any colloid-catalysed hydrogenation would result in no or very low enantioselective discrimination. However, if cluster fragmentation occurs, the formation of mononuclear chiral diphosphine complexes that can lead to effective enantioselective hydrogenation can not be excluded. In this investigation, the building blocks for a Noyori-type catalyst with the general formula [Ru<sup>II</sup>(P-P)(O<sub>2</sub>CR)<sub>2</sub>]<sup>[39]</sup> are present in the reaction systems; however, the formation of such a catalytic species would require oxidation of the metal. To investigate the possibility that such a Noyori-type catalyst is formed, and to compare the enantioselectivities of such catalysts to those obtained with the present cluster-based catalysts, the ruthenium complexes [Ru<sup>II</sup>{(*R*)-BINAP}(OAc)<sub>2</sub>] (**22**) ((*R*)-BINAP = (*R*)-(+)-2,2'-bis(diphenylphosphino)-1,1'-binaphthyl) and [Ru<sup>II</sup>{(*R,R*)-**2a**}(OAc)<sub>2</sub>] (**23**) were prepared by using the synthetic route described by Noyori et al.<sup>[39]</sup> The catalytic

activity of the two mononuclear complexes **22** and **23** was investigated by hydrogenation of tiglic acid (**24**) under the same reaction conditions used for the cluster-based catalysts. Both complexes **22** and **23** proved to be efficient catalysts (see Table 7 entries 48 and 49) with good substrate conversion but formed more byproducts than the cluster-based catalysts. The observed enantioselectivities were significantly different from those obtained by using the corresponding cluster-based catalyst. Thus, complex **22** yielded an *ee* of 68% (*R*), exceeding the *ees* reported for [H<sub>4</sub>Ru<sub>4</sub>(CO)<sub>10</sub>{(*S*)-BINAP}] under similar conditions<sup>1</sup> by more than forty percentage units. In contrast, complex **23** generated an enantiomeric excess of 30% (*S*), which is more than fifty percentage units less than that of complex **12**. These results indicate that mononuclear Noyori-type catalysts are not the catalytically active species in the cluster-based reactions.

In addition to the above-mentioned studies, a series of NMR experiments by using a mixture of hydrogen enriched in the para isomer form (parahydrogen, p-H<sub>2</sub>) were carried out in order to utilise the parahydrogen-induced polarisation (PHIP) effect<sup>[40]</sup> to detect low concentration species (i.e., catalytic cycle intermediates). Several examples of parahydrogen addition to transition-metal clusters have been reported previously,<sup>[41]</sup> including studies of catalytic hydrogenation systems.<sup>[41e-g]</sup> However, signals due to the PHIP effect could neither be detected for the reaction of [H<sub>4</sub>Ru<sub>4</sub>(CO)<sub>10</sub>(μ-1,2-**2a**)] (**12**) with a parahydrogen-enriched mixture, nor for the hydrogenation of (*E*)-2-methyl-2-butenoic acid (tiglic acid) (**24**) by using parahydrogen (see the Supporting Information).

**Turnover number and turnover frequency:** In an attempt to establish a turnover number (TON) for catalyst **12**, a molar substrate (**24**)/catalyst/Hg ratio of 10000:1:16000 was used, and the reaction mixture was heated for 96 h. <sup>1</sup>H/<sup>31</sup>P NMR and IR spectroscopic analyses showed no other cluster species than **12** present in the reaction mixture upon completion of the experiment. The substrate/product ratios were assessed by <sup>1</sup>H NMR spectroscopy and gave the following result: tiglic acid (0.5%), 2-methylbutanoic acid (87%) and ethyl 2-methylbutanoate (12.5%); the TON can thus be considered to be >9900. The enantiomeric excess of the isolated product 2-methylbutanoic acid was determined to be 87% (*S*). The results from this experiment show that the enantioselectivity in this catalytic system is retained even when quite high substrate/catalyst ratios are used (see Table 7, entry 6).

Our experimental setup has precluded sampling during the reaction, but in order to establish an understanding of the catalytic efficiency of complex **12**, a set of time-dependent experiments was carried out to determine the turn over frequency (TOF). A catalyst/substrate ratio of 1:1000 was used, and reaction times were set to 3, 6, 12 and 24 h. The

<sup>1</sup> Reaction conditions used (see Ref. [14b]): *T* = 100 °C, duration = 93 h, solvent = ethanol/toluene (1:1 v/v, 20 mL), pressure H<sub>2</sub> = 130 bar, molar ratio substrate/catalyst = 2000. Results obtained: conversion = 90.5%, optical purity = 28.5% *ee* (*R*).

results for these reactions are presented in Table 8, and indicate that cluster **12** is quite reactive. The results show that under the conditions used, the standard reaction time of

Table 8. Results from turn over frequency tests of  $[\text{H}_4\text{Ru}_4(\text{CO})_{10}(\mu\text{-}1,2\text{-}\mathbf{2a})]$  (**12**) used in the hydrogenation of tiglic acid (**24**).

Time [h]	Conversion <sup>[a]</sup> [%]	Time [h]	Conversion <sup>[a]</sup> [%]
3	14	12	95
6	92	24	99

[a] Conversion of substrate assessed with  $^1\text{H}$  NMR spectroscopy.

24 h is unnecessarily long when cluster **12** is used to hydrogenate tiglic acid, but they do prove that the catalyst/catalyst precursor is stable for a prolonged time under heat and pressure. However, the results from this investigation imply that there is an induction time of approximately 3 h (or less). This behaviour is usually seen in catalytic systems where the homogeneous catalyst is transformed into a heterogeneous/colloidal catalyst during the induction time, after which the reaction starts. An experiment was performed to investigate this issue. In an identical catalytic test, the pressurised reactor was allowed to “equilibrate” for 3 h before it was heated to 100 °C for another 3 h. The pre-equilibration step did improve the conversion by ten percentage units relative to three hours of reaction without pre-equilibration, so that 24 % of the substrate was hydrogenated.

In order to investigate this further, a high-pressure NMR analysis was performed by using a high-pressure sapphire tube (5.0 mm o.d./3.4 mm i.d.).<sup>[42]</sup> A saturated solution of cluster **12** in  $[\text{D}_8]$ toluene (0.4 mL) was prepared and added to the tube. A reference spectrum was recorded at 298 K before the tube was pressurised with 20 bar of hydrogen gas. The pressurised NMR sample was given 48 h to equilibrate before any measurements were carried out. In addition to the hydrides typical for cluster **12**, the new NMR spectrum collected in the hydride region showed the presence of a new signal at  $\delta = -17.67$  ppm (see Figure 22). Proton spectra were recorded at 60 and 80 °C. In comparison to the variable-temperature  $^1\text{H}$  NMR spectroscopy (see Figure 5) performed under normal atmospheric pressure of  $\text{N}_2$ , the pressurised sample exhibits three sharp hydride resonances, whereas the “normal” pressure sample shows two sharp ( $\delta = -16.71$  and  $-17.15$  ppm) and two broad signals ( $\delta = -16.21$  and  $-18.02$  ppm). At 80 °C the pressurised cluster sample shows a sharp and a broad signal, and four resonances significantly weaker. In contrast, the normal pressure sample shows one sharp ( $\delta = -17.09$  ppm) and one broad ( $\delta = -16.86$  ppm) resonance together with a resonance of weak intensity ( $\delta = -16.50$  ppm). No darkening of the solution or metallic precipitation was observed, indicating that cluster fragmentation did not occur during this experiment.

A kinetic study by Doi et al.<sup>[43]</sup> has shown that the parent cluster  $[\text{H}_4\text{Ru}_4(\text{CO})_{12}]$  hydrogenates ethene in heptane at 72 °C under hydrogen pressures of 0.1–0.4 bar. It has been demonstrated that evolution of carbon monoxide occurs when a solution of  $[\text{H}_4\text{Ru}_4(\text{CO})_{12}]$  in heptane is exposed to

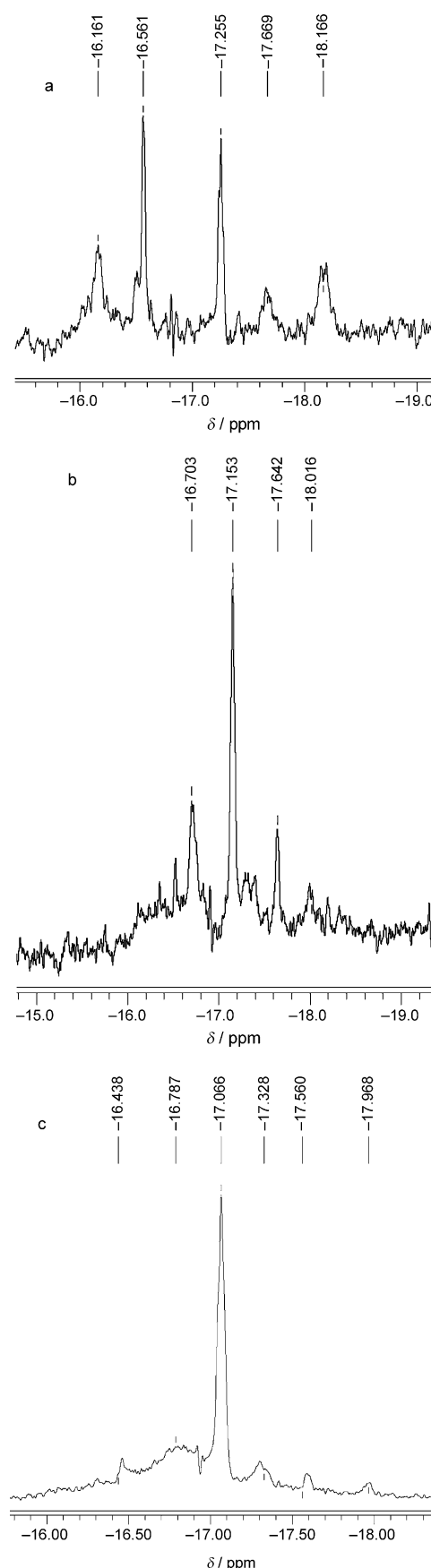


Figure 22.  $^1\text{H}$  NMR spectra of  $[\text{H}_4\text{Ru}_4(\text{CO})_{10}(\mu\text{-}1,2\text{-}\mathbf{2a})]$  (**12**) under 20 bar  $\text{H}_2$  pressure at a) 298, b) 333 and c) 353 K.

hydrogen<sup>[43,44]</sup> and the suppression of catalysis by addition of CO<sup>[43,44]</sup> suggests initial decarbonylation of the cluster and formation of  $[\text{H}_4\text{Ru}_4(\text{CO})_{11}(\text{alkene})]$  and, subsequently,  $[\text{H}_3\text{Ru}_4(\text{CO})_{11}(\text{alkyl})]$  species.<sup>[15,43]</sup> Doi et al.<sup>[43]</sup> have proposed that the initial coordination of the alkene occurs in competition with coordination of  $\text{H}_2$  to form the hexahydrido species  $[\text{H}_6\text{Ru}_4(\text{CO})_{11}]$  and it may be such a species that is detected in the above-mentioned high-pressure NMR experiment under  $\text{H}_2$  pressure, which takes place in the absence of substrate. We have attempted the catalytic reduction of tiglic acid (**24**) by  $[\text{H}_4\text{Ru}_4(\text{CO})_{10}(\mu\text{-}1,2\text{-}\mathbf{2a})]$  (**12**) under the conditions used by Doi et al.<sup>[43]</sup> but no conversion could be detected after 14 h; again, the hydrogen pressure (and/or the temperature) appears to be too low to enable hydrogenation of the substrate. It should be mentioned that an alternative catalytic pathway<sup>[15]</sup> involves an initial step where a metal–metal bond rupture leads to the formation of a two-electron-deficient 60-electron butterfly cluster followed by coordination of the substrate. This alternative reaction pathway does not require ligand dissociation, but would probably still be susceptible to competitive reactions, that is, the association of either the substrate or dihydrogen.

In an attempt to further monitor the reaction system under catalytic conditions, a high-pressure IR spectroscopy experiment was conducted. Cluster **12** (20 mg) was dissolved in an ethanol/toluene mixture (1:1 v/v, 20 mL) and heated to 100 °C at a total hydrogen pressure of 50 bar. However, no change could be observed in the carbonyl region and the experiment was terminated after 5 h of heating. The sample was left under pressure for another 15 h at ambient temperature, but no change in the spectrum could be seen. In another experiment, cluster **12** and substrate **24** ( $n_{\text{catalyst}}/n_{\text{substrate}}$  1:100) were dissolved in cyclohexane and heated to 100 °C under a hydrogen pressure of 50 bar. No detection of any other cluster species than **12** could be observed during the experiment lasting six hours. This experiment provides further evidence of the stability of cluster **12** under catalytic conditions, suggesting that the cluster may indeed be the active catalyst, or a direct precursor for an active cluster catalyst.

## Conclusion

In summary, we have synthesised and characterised new tetraruthenium clusters, derivatised with chiral ferrocenyl-based diphosphine ligands and used these clusters as catalysts for asymmetric hydrogenation of  $\alpha$ -unsaturated carboxylic acids. The catalytic activities for certain clusters reported here outclass all previous attempts to effect the enantioselectivity in asymmetric hydrogenation by using  $[\text{H}_4\text{Ru}_4(\text{CO})_{10}(\text{diphosphine})]$  clusters as catalysts. Furthermore, the results obtained in this investigation clearly demonstrate the importance of the chiral ligand used. Although it has not been possible to unambiguously determine the nature of the active catalyst(s) in these cluster-based systems, the clusters in this study that exhibit good catalytic ef-

iciency offer several distinct advantages: they are robust and are not air sensitive, separation from the products is relatively facile and they permit low catalyst-to-substrate ratios.

## Experimental Section

**General:** All reactions were performed under inert atmosphere (nitrogen or argon) and manipulations of the products were performed in air. The reactions were performed at room temperature ( $\approx 21$  °C) unless stated otherwise. All solvents used in syntheses and catalysis experiments were distilled and dried prior to use. The parent cluster  $[\text{H}_4\text{Ru}_4(\text{CO})_{12}]$  was prepared according to a literature method.<sup>[1,45]</sup>  $^1\text{H}$  and  $^{31}\text{P}$  NMR spectra were recorded on a Varian Unity 300 MHz spectrometer, a Varian Inova 500 MHz spectrometer or a JEOL EX-400 MHz spectrometer. The  $^1\text{H}$  NMR spectra were referenced to the relevant resonances of the non-deuterated solvents ( $\text{CHCl}_3$ ,  $\delta = 7.25$  ppm;  $\text{CH}_2\text{Cl}_2$ ,  $\delta = 5.31$  ppm; toluene,  $\delta = 2.09$  ppm; benzene,  $\delta = 7.15$  ppm).  $^{31}\text{P}$  NMR shifts were referenced to external  $\text{H}_3\text{PO}_4$  (85 %). Infrared spectra were recorded on a Nicolet Avatar 360 FTIR spectrometer. Thin-layer chromatography was performed on commercially available  $20 \times 20$  cm glass plates, covered with Merck Kieselgel 60 to 0.25 mm thickness.

A number of prototypical syntheses for the different structural types of Josiphos- and Walphos-containing clusters (see Table 3) are described below. Full documentation of synthetic and spectroscopic data for the remaining new clusters can be found in the Supporting Information.

**Synthesis of  $[\text{H}_4\text{Ru}_4(\text{CO})_{10}(1,1\text{-}\mathbf{1a})]$  (**3**) and  $[\text{H}_4\text{Ru}_4(\text{CO})_{10}(\mu\text{-}1,2\text{-}\mathbf{1a})]$  (**4**):**  $[\text{H}_4\text{Ru}_4(\text{CO})_{12}]$  (23 mg, 31  $\mu\text{mol}$ ) and (*R*)-1-[(*S*)-2-(diphenylphosphino)ferrocenyl]ethylidicyclohexylphosphine (**1a**) (20 mg, 31  $\mu\text{mol}$ ) were dissolved in a solvent mixture of dichloromethane (25 mL) and acetonitrile (10 mL). Under vigorous stirring, a small excess of  $\text{Me}_3\text{NO}$  (4 mg, 36  $\mu\text{mol}$ ) dissolved in acetonitrile (15 mL) was added dropwise to the orange cluster/ligand solution, which instantly started to change colour towards red. After 3 h the solvents were removed under reduced pressure. The red solid residue obtained was dissolved in a small quantity of dichloromethane and purified by using preparative TLC ( $\text{CH}_2\text{Cl}_2/n\text{-hexane}$  3:2 v/v). Except for traces of starting materials and one stationary brown band (decomposed material), two bands were isolated from the TLC plates and extracted with  $\text{CH}_2\text{Cl}_2$  and dried under vacuum. The two solids obtained, orange and red, were identified as  $[\text{H}_4\text{Ru}_4(\text{CO})_{10}(1,1\text{-}\mathbf{1a})]$  (**3**) (4 mg, 10 %);  $^1\text{H}$  NMR (hydride resonances, 500 MHz,  $\text{CDCl}_3$ ):  $\delta = -16.0$  (ddd,  $J = 32.7, 15.0, 2.6$  Hz),  $-16.4$  (s),  $-17.7$  (t,  $J = 24.4$  Hz),  $-18.9$  ppm (dt,  $J = 8.6, 2.4$  Hz);  $^{31}\text{P}\{^1\text{H}\}$  NMR (202 MHz,  $\text{CDCl}_3$ ):  $\delta = 63.5, 23.4$  ppm; IR ( $\text{CH}_2\text{Cl}_2$ ):  $\tilde{\nu}_{\text{CO}} = 2072$  (s), 2041 (vs), 2018 (vs), 1997 (s), 1977 (s), 1977 (br), 1965  $\text{cm}^{-1}$  (br); MS (FAB):  $m/z$ : 1284  $[M]^+$ ; and  $[\text{H}_4\text{Ru}_4(\text{CO})_{10}(\mu\text{-}1,2\text{-}\mathbf{1a})]$  (**4**) (24 mg, 60 %)  $^1\text{H}$  NMR (hydride resonances, 500 MHz,  $\text{CDCl}_3$ ):  $\delta = -16.6$  (sbr),  $-17.3$  (sbr),  $-17.7$  (sbr),  $-18.0$  ppm (sbr);  $^{31}\text{P}\{^1\text{H}\}$  NMR (202 MHz,  $\text{CDCl}_3$ ):  $\delta = 65.8, 32.1$  ppm; IR ( $\text{CH}_2\text{Cl}_2$ ):  $\tilde{\nu}_{\text{CO}} = 2065$  (s), 2044 (s), 2022 (vs), 2001 (s), 1990 (br), 1979 (br), 1956  $\text{cm}^{-1}$  (br); MS (FAB):  $m/z$ : 1283  $[M-1]^+$ .

**Synthesis of  $[\text{H}_4\text{Ru}_4(\text{CO})_{10}(1,1\text{-}\mathbf{2a})]$  (**11**) and  $[\text{H}_4\text{Ru}_4(\text{CO})_{10}(\mu\text{-}1,2\text{-}\mathbf{2a})]$  (**12**)**

**Method A (oxidative decarbonylation/ligand substitution):** An excess of  $\text{Me}_3\text{NO}$  (8 mg, 72  $\mu\text{mol}$ ) dissolved in methanol (5 mL) was added dropwise to a stirred solution of (*R*)-1-[(*R*)-2-(2'-diphenylphosphinophenyl)ferrocenyl]ethylidibis-(3,5-trifluoromethyl)phenyl]phosphine (**2a**) (40 mg, 43  $\mu\text{mol}$ ) and  $[\text{H}_4\text{Ru}_4(\text{CO})_{12}]$  (18 mg, 24  $\mu\text{mol}$ ) in benzene (20 mL) over a period of 20 min. During the addition of  $\text{Me}_3\text{NO}$ , the colour of the solution changed gradually from orange to deep red. After 5 h the solvent was removed under vacuum and the red solid obtained was dissolved in a small volume of  $\text{CH}_2\text{Cl}_2$  ( $\approx 2$  mL), and purified by using preparative TLC (eluent: hexane/ $\text{CH}_2\text{Cl}_2$  1:1 v/v). Except for traces of unreacted ligand and a stationary brown band, two new products were observed and identified as  $[\text{H}_4\text{Ru}_4(\text{CO})_{10}(1,1\text{-}\mathbf{2a})]$  (**11**) (3 mg, 7 %);  $^1\text{H}$  NMR (hydride resonances, 500 MHz,  $\text{CDCl}_3$ ):  $\delta = -15.67$  (s),  $-15.97$  (s),  $-16.51$

(m br),  $-16.75$  ppm (s);  $^{31}\text{P}\{^1\text{H}\}$  NMR (202 MHz,  $\text{CDCl}_3$ ):  $\delta=43.32$  (s),  $4.34$  ppm (s); IR ( $\text{CH}_2\text{Cl}_2$ ):  $\tilde{\nu}_{\text{CO}}=2078$  (s),  $2049$  (s),  $2027$  (vs),  $2003$  (m),  $1983$  (m, sh),  $1965$  (v, sh),  $1949$   $\text{cm}^{-1}$  (v sh); MS (FAB):  $m/z$ :  $1620$  [ $M$ ] $^+$ ; and  $[\text{H}_4\text{Ru}_4(\text{CO})_{10}(\mu\text{-}1,2\text{-}\mathbf{2a})]$  ( $\mathbf{12}$ ) (17 mg, 43 %);  $^1\text{H}$  NMR (hydride resonances, 500 MHz,  $\text{CDCl}_3$ ):  $\delta=-16.4$  (m br),  $-16.7$  (d,  $J=7.3$  Hz),  $-17.6$  (td,  $J=11$ ,  $J=2.4$  Hz),  $-18.5$  ppm (br m,  $J\approx 30$  Hz);  $^{31}\text{P}\{^1\text{H}\}$  NMR (202 MHz,  $\text{CDCl}_3$ ):  $\delta=45.9$  (m),  $39.1$  ppm (m); IR ( $\text{CH}_2\text{Cl}_2$ ):  $\tilde{\nu}_{\text{CO}}=2073$  (ms),  $2053$  (ms),  $2028$  (vs),  $2013$  (s),  $1998$  (w),  $1965$   $\text{cm}^{-1}$  (w); MS (FAB):  $m/z$ :  $1620$  [ $M$ ] $^+$ . Single crystals suitable for X-ray diffraction analysis were obtained by re-crystallisation from a dichloromethane/hexane/methanol solution.

#### Synthesis of $[\text{H}_4\text{Ru}_4(\text{CO})_{10}(\mu\text{-}1,2\text{-}\mathbf{2a})]$ ( $\mathbf{12}$ )

**Method B (thermal ligand substitution at high-pressure):** In a high-pressure autoclave,  $[\text{H}_4\text{Ru}_4(\text{CO})_{12}]$  (30 mg,  $42$   $\mu\text{mol}$ ) and  $\mathbf{2a}$  (50 mg,  $54$   $\mu\text{mol}$ ) were suspended in benzene (10 mL). The autoclave was assembled and pressurised with  $\text{H}_2$ , (25 bar) after being purged with  $\text{H}_2$  ( $3\times 10$  bar). The autoclave was heated at  $100^\circ\text{C}$  for 4 h, after which it was allowed to cool to room temperature. The autoclave was opened and the solvent of the reaction mixture was removed by using rotary evaporation. The resultant red solid was dissolved in a minimum quantity of  $\text{CH}_2\text{Cl}_2$  and filtered through a short plug of Merck Kieselgel 60. The red solid obtained after concentration under vacuum was identified as  $[\text{H}_4\text{Ru}_4(\text{CO})_{10}(\mu\text{-}1,2\text{-}\mathbf{2a})]$  ( $\mathbf{12}$ ) (50 mg, 73 %).

#### Synthesis of $[\text{H}_4\text{Ru}_4(\text{CO})_{11}(\mathbf{2a})]$ ( $\mathbf{13}$ )

**Method A (oxidative decarbonylation/ligand substitution):** A small excess of  $\text{Me}_3\text{NO}$  (5.4 mg,  $50$   $\mu\text{mol}$ ) dissolved in methanol (5 mL) was added dropwise to a stirred solution of  $\mathbf{2a}$  (40 mg,  $43$   $\mu\text{mol}$ ) and  $[\text{H}_4\text{Ru}_4(\text{CO})_{12}]$  (18 mg,  $24$   $\mu\text{mol}$ ) in benzene (20 mL) over a period of 20 min. During the addition of  $\text{Me}_3\text{NO}$  the colour of the solution changed gradually from orange to deep red. After 40 min the solvent was removed under vacuum and the red solid obtained was dissolved in a small volume of  $\text{CH}_2\text{Cl}_2$  ( $\approx 2$  mL), and purified by using preparative TLC (eluent: hexane/ $\text{CH}_2\text{Cl}_2$  1:1 v/v). Except for a stationary brown band (decomposed material), two new products were observed and identified as  $[\text{H}_4\text{Ru}_4(\text{CO})_{11}(\mathbf{2a})]$  ( $\mathbf{13}$ ) (17 mg, 44 %);  $^1\text{H}$  NMR (hydride resonances, 500 MHz,  $\text{CDCl}_3$ ):  $\delta=-17.14$  ppm (s);  $^{31}\text{P}\{^1\text{H}\}$  NMR (202 MHz,  $\text{CDCl}_3$ ):  $\delta=38.90$  (s),  $4.68$  ppm (s); IR ( $\text{CH}_2\text{Cl}_2$ ):  $\tilde{\nu}_{\text{CO}}=2094$  (w),  $2086$  (m),  $2061$  (vs),  $2053$  (vs),  $2031$  (vs),  $2007$  (s),  $1990$  (m),  $1963$   $\text{cm}^{-1}$  (w); MS (FAB):  $m/z$ :  $1650$  [ $M+2$ ] $^+$ ; and  $\mathbf{12}$  (8 mg, 20 %). Single crystals suitable for X-ray analysis were grown from a dichloromethane/hexane/methanol solution.

**Synthesis of  $[\text{Ru}^{\text{II}}(\text{R})\text{-BINAP}(\text{OAc})_2]$  ( $\mathbf{22}$ ) and  $[\text{Ru}^{\text{II}}(\mathbf{2a})(\text{OAc})_2]$  ( $\mathbf{23}$ ):** Compounds  $\mathbf{22}$  and  $\mathbf{23}$  were prepared according to a literature method.<sup>[39]</sup> Triethylamine (72  $\mu\text{L}$ ,  $0.51$  mmol) was added to a solution of  $[\text{RuCl}_2(\text{COD})]$  (COD=cyclooctadiene) (28 mg,  $0.1$  mmol) and  $\mathbf{2a}$  (100 mg,  $0.1$  mmol) in toluene (5 mL). The mixture was heated to reflux for 12 h and the colour of the solution changed from yellow-brown to transparent orange-brown. The reaction mixture was allowed to cool to ambient temperature and the solvent was removed under vacuum. The resultant brownish solid residue was dissolved in dichloromethane, filtered through a short plug of celite and concentrated under vacuum. The solid residue was dissolved in *tert*-butanol (5 mL) and anhydrous sodium acetate (40 mg,  $0.5$  mmol) was added. The mixture was heated to reflux for 12 h. Once the reaction mixture reached ambient temperature, the solvent was removed under vacuum, and the solid residue was extracted with diethyl ether ( $3\times 3$  mL) and concentrated under vacuum. The resulting solid was extracted with ethanol ( $3\times 3$  mL) and evaporation of the solvent under vacuum afforded a yellow-brown solid identified as  $[\text{Ru}^{\text{II}}(\mathbf{2a})(\text{OAc})_2]$  ( $\mathbf{23}$ ) (35 mg, 32 %);  $^{31}\text{P}\{^1\text{H}\}$  NMR (202 MHz,  $\text{CDCl}_3$ ):  $\delta=93.2$  (s br),  $86.9$  ppm (s br); IR ( $\text{CH}_2\text{Cl}_2$ ):  $\tilde{\nu}_{\text{CO}}=1572$  (m),  $1463$   $\text{cm}^{-1}$  (m).

**Electrochemistry:** Cyclic voltammetry was performed at ambient temperature by using a Bioanalytical Systems Inc. BAS 100W Electrochemical Analyser with a one-compartment three-electrode system comprising a platinum disk working electrode, a platinum wire auxiliary electrode and a  $\text{Ag}/\text{Ag}^+$  reference electrode (0.01 M  $\text{AgNO}_3$  and 0.1 M  $[\text{nBu}_4\text{N}][\text{ClO}_4]$  in anhydrous acetonitrile). The reported  $E$  values (see Table 6) are with reference to this electrode. Measurements were made on anhydrous acetonitrile solutions that were 2 mm in sample and contained 0.1 M  $[\text{nBu}_4\text{N}][\text{ClO}_4]$  as background electrolyte. Unless otherwise stated, the

scan rate used was  $100$   $\text{mV s}^{-1}$ . Under these conditions the ferrocene/ferrocenium couple, which was used as a reference, had an  $E_{1/2}$  value of  $+0.09$  V and  $\Delta E_p=120$  mV. All solutions were purged with argon and voltammograms were recorded under a blanket of argon. The platinum disk working electrode was polished between runs.

**Catalysis experiments:** In a typical catalytic experiment, a mini bench autoclave (Carl Roth, 100 mL) was charged with (cluster) catalyst (10 mg) and substrate (250 or 1000 molar excess) under inert atmosphere. A degassed toluene/ethanol mixture (5–6 mL, 1:1 v/v) was added. The reaction vessel was closed and purged with hydrogen gas ( $4\times 20$  bar) before final pressurising to 50 bar. The reaction mixture was continuously stirred with a magnetic stirrer ( $\approx 800$  rpm) and heated to  $100^\circ\text{C}$  for 24 h. The autoclave was allowed to cool to ambient temperature before the hydrogen gas was cautiously released. The reaction mixture was transferred to a round bottom flask and concentrated under vacuum. The conversions for the catalysis runs were calculated on the basis of NMR analyses. To separate the carboxylic acid from the cluster, the reaction residue was dissolved in diethyl ether (10 mL) and the carboxylic acid was extracted with aqueous sodium hydroxide solution (1 M,  $3\times 10$  mL) and washed with diethyl ether ( $2\times 5$  mL), leaving the cluster in the organic solvent. The carboxylate was protonated with sulfuric acid (conc., q.s.), extracted with diethyl ether ( $3\times 10$  mL), washed with water ( $2\times 5$  mL) and dried over magnesium sulfate. The ether was removed under vacuum, yielding the carboxylic acid quantitatively. The ether phase, from which the carboxylic acid was extracted, was concentrated under vacuum to recover the remaining cluster. In certain cases, where ester formation was observed during the catalytic experiment, the recovered cluster was dissolved in a minimum quantity of dichloromethane and the products were separated by using preparative TLC, eluting with hexane/dichloromethane (1:1 v/v). Usually 60–70 % of the cluster was recovered after a catalytic run, and was analysed by IR and NMR spectroscopy.

The enantiomeric excess of the product was determined by converting the reduced carboxylic acid with (*S*)-mandelate and analysing the diastereomeric mixture by NMR spectroscopy, as described by Tyrell et al.<sup>[46]</sup> It was found that flash chromatography of the final product(s) was not necessary.

**Catalyst poisoning test by using mercury:** The experimental setup followed the procedure described above for catalytic experiments, except that metallic mercury (ca. 2 g) was added to the reaction mixture before the autoclave was sealed and pressurised. After a complete catalytic run, the Hg had acquired a faint grey film on some parts of its surface. Products were separated and analysed as mentioned above.

**Determination of the TON:** In a bench autoclave (Parr instruments, 450 mL)  $[\text{H}_4\text{Ru}_4(\text{CO})_{10}(\mu\text{-}1,2\text{-}\mathbf{2a})]$  ( $\mathbf{12}$ ) (10 mg,  $6.18$   $\mu\text{mol}$ ) and tiglic acid (6.056 g,  $60.6$  mmol) were dissolved in an ethanol/toluene mixture (60 mL, 1:1 v/v) in the presence of metallic mercury (20.03 g,  $0.1$  mol). The reaction vessel was sealed and purged several times before being pressurised with  $\text{H}_2$  (50 bar). The autoclave was heated at  $100^\circ\text{C}$  under continuous stirring for 96 h. It was then cooled down to room temperature before carefully opened, and the products were separated and analysed as described above for the catalytic experiments.

**Control experiment with ligand  $\mathbf{2a}$  and tiglic acid:** In a small autoclave,  $\mathbf{2a}$  (10 mg,  $10.7$   $\mu\text{mol}$ ) and tiglic acid (263 mg,  $2.7$  mmol) were dissolved in an ethanol/toluene mixture (5 mL, 1:1 v/v). The autoclave was sealed and purged with  $\text{H}_2$  ( $3\times 15$  bar) before being pressurised with  $\text{H}_2$  (50 bar) and heated to  $100^\circ\text{C}$  for 78 h. Products were separated and analysed as described above for the catalytic experiments.

**NMR measurements:** All NMR solvents (Aldrich) were used as received. The NMR measurements were made by using 5 mm (o.d.) tubes fitted with J. Young Teflon valves. Typically approximately 0.5 mL of a saturated [ $\text{D}_2$ ]dichloromethane solution of  $[\text{H}_4\text{Ru}_4(\text{CO})_{10}(\mu\text{-}1,2\text{-}\mathbf{2a})]$  ( $\mathbf{12}$ ) was added and the tube was sealed under  $\text{N}_2$  atmosphere. For high-temperature NMR studies, [ $\text{D}_8$ ]toluene was used as solvent. The EXSY experiment<sup>[47]</sup> was performed by using standard parameters. The mixing time was selected to be 0.5 s. The  $^1\text{H},^{31}\text{P}$  HetCor experiment was performed with a solution of  $\mathbf{12}$  in [ $\text{D}_3$ ]chloroform at 223 K.

High-pressure NMR measurements were carried out in a 5 mm (o.d.) sapphire tube, which was charged with 0.3 mL of a saturated solution of

Table 9. Crystallographic data for clusters **4**, **7–9**, **12**, **13**, **15**, **17** and **19–21**.

	<b>4</b>	<b>7</b>	<b>8</b>	<b>9</b>	<b>12</b>	<b>13</b>
formula	C <sub>46</sub> H <sub>48</sub> FeO <sub>10</sub> P <sub>2</sub> Ru <sub>4</sub>	C <sub>46</sub> H <sub>40</sub> FeO <sub>10</sub> P <sub>2</sub> Ru <sub>4</sub>	C <sub>47</sub> H <sub>62</sub> Cl <sub>2</sub> FeO <sub>10</sub> P <sub>2</sub> Ru <sub>4</sub>	C <sub>50</sub> H <sub>44</sub> FeO <sub>10</sub> P <sub>2</sub> Ru <sub>4</sub>	C <sub>62</sub> H <sub>50</sub> F <sub>12</sub> Fe O <sub>10</sub> P <sub>2</sub> Ru <sub>4</sub>	C <sub>58</sub> H <sub>38</sub> Cl <sub>2</sub> F <sub>12</sub> FeO <sub>11</sub> P <sub>2</sub> Ru <sub>4</sub>
<i>M<sub>r</sub></i>	1282.91	1295.01	1379.94	1326.92	1705.09	1731.85
<i>T</i> [K]	100(2)	120(2)	120(2)	120(2)	100(2) K	120(2)
<i>λ</i> [Å]	0.71073	0.71073	0.71073	0.71073	0.71073	0.71073
crystal system	orthorhombic	monoclinic	monoclinic	orthorhombic	monoclinic	orthorhombic
space group	<i>P</i> 2 <sub>1</sub> 2 <sub>1</sub> 2 <sub>1</sub>	<i>P</i> 2 <sub>1</sub>	<i>P</i> 2 <sub>1</sub>	<i>P</i> 2 <sub>1</sub> 2 <sub>1</sub> 2 <sub>1</sub>	<i>C</i> <sub>2</sub>	<i>P</i> 2 <sub>1</sub> 2 <sub>1</sub> 2 <sub>1</sub>
<i>a</i> [Å]	12.3611(2)	10.3579(4)	10.79530(10)	11.0794(2)	44.368(9)	13.02990(10)
<i>b</i> [Å]	16.7583(2)	20.9527(11)	21.0136(2)	19.1761(3)	10.745(2)	15.0032(2)
<i>c</i> [Å]	23.1317(3)	12.0081(10)	11.66880(10)	23.1694(3)	14.356(3)	32.0496(5)
<i>β</i> [°]	90	110.280(5)°	99.979(8)°	90	103.65(3)°	90
<i>V</i> [Å <sup>3</sup> ]	4791.76(11)	2444.5(3)	2607.00(4)	4922.56(13)	6651(2)	6265.38(14)
<i>Z</i>	4	2	2	4	4	4
<i>ρ</i> <sub>calcd</sub> [g cm <sup>-3</sup> ]	1.778	1.759	1.758	1.790	1.703	1.836
<i>μ</i> [mm <sup>-1</sup> ]	1.649	1.617	1.621	1.609	1.236	1.398
crystal size [mm]	0.32 × 0.22 × 0.06	0.28 × 0.27 × 0.26	0.61 × 0.35 × 0.32	0.57 × 0.22 × 0.10	0.26 × 0.23 × 0.08	0.22 × 0.19 × 0.06
<i>θ</i> limits [°]	2.94 to 27.53	2.66 to 27.50	2.99 to 27.47	3.52 to 27.47	2.10 to 27.50	2.98 to 26.50
<i>h</i> range	−14 to 16	−12 to 13	−13 to 14	−14 to 12	−57 to 57	−16 to 15
<i>k</i> range	−21 to 21	−27 to 27	−27 to 27	−24 to 18	−13 to 13	−18 to 18
<i>l</i> range	−27 to 30	−15 to 15	−14 to 15	−29 to 28	−18 to 18	−40 to 38
reflns collected	47056	32047	31635	32325	40378	42090
independent reflns	10952	10772	11524	10629	15198	12963
data/restraints/	10952/0/585	10772/1/585	11524/1/612	10629/0/625	15198/1/793	12963/56/830
parameters						
goodness-of-fit on <i>F</i> <sup>2</sup>	1.057	1.022	1.046	1.069	1.015	1.033
<i>R</i> 1 <sup>[a]</sup>	0.0230	0.0169	0.0219	0.0218	0.0280	0.0357
<i>wR</i> 2 <sup>[a]</sup>	0.0459	0.0323	0.0567	0.0477	0.0634	0.0745
weighting scheme	<i>x</i> = 0.0195 <i>y</i> = 0.0570	<i>x</i> = 0.0120 <i>y</i> = 0.1866	<i>x</i> = 0.0274 <i>y</i> = 2.619	<i>x</i> = 0.0230 <i>y</i> = 0.7241	<i>x</i> = 0.0370 <i>y</i> = 5.7466	<i>x</i> = 0.0376 <i>y</i> = 2.8402
largest diff. peak/ hole [e Å <sup>-3</sup> ]	0.543/−0.592	0.590/−0.321	1.142/−1.187	0.410/−0.727	0.946/−0.770	0.980/−0.832
Flack parameter	−0.033(13)	−0.002(9)	−0.008(13)	−0.014(12)	−0.003(13)	0.008(18)
	<b>15</b>	<b>17</b>	<b>19</b>	<b>20</b>	<b>21</b>	
formula	C <sub>52</sub> H <sub>40</sub> FeO <sub>10</sub> P <sub>2</sub> Ru <sub>4</sub>	C <sub>52</sub> H <sub>52</sub> FeO <sub>10</sub> P <sub>2</sub> Ru <sub>4</sub>	C <sub>58</sub> H <sub>51</sub> FeNO <sub>10</sub> P <sub>2</sub> Ru <sub>4</sub>	C <sub>57</sub> H <sub>50</sub> Cl <sub>2</sub> F <sub>12</sub> FeO <sub>10</sub> P <sub>2</sub> Ru <sub>4</sub>	C <sub>61</sub> H <sub>38</sub> Cl <sub>2</sub> Fe O <sub>10</sub> P <sub>2</sub> Ru <sub>4</sub>	
<i>M<sub>r</sub></i>	1346.91	1359.01	1444.07	1715.94	1544.04	
<i>T</i> [K]	120(2)	120(2)	120(2)	120(2)	120(2)	
<i>λ</i> [Å]	0.71073	0.71073	0.71073	0.71073	0.71073	
crystal system [mm]	orthorhombic	monoclinic	orthorhombic	orthorhombic	monoclinic	
space group	<i>P</i> 2 <sub>1</sub> 2 <sub>1</sub> 2 <sub>1</sub>	<i>P</i> 2 <sub>1</sub>	<i>P</i> 2 <sub>1</sub> 2 <sub>1</sub> 2 <sub>1</sub>	<i>P</i> 2 <sub>1</sub> 2 <sub>1</sub> 2 <sub>1</sub>	<i>P</i> 2 <sub>1</sub> / <i>n</i>	
<i>a</i> [Å]	10.836(2)	11.6004(2)	11.48040(10)	12.18500(10)	11.2410(2)	
<i>b</i> [Å]	14.243(3)	17.8442(5)	19.9411(4)	20.0480(4)	20.8736(5)	
<i>c</i> [Å]	32.129(6)	12.3817(3)	24.9251(5)	25.4160(5)	26.4175(4)	
<i>β</i> [°]	90	93.325(2)°	90	90	95.2970(10)°	
<i>V</i> [Å <sup>3</sup> ]	4958.9(17)	2558.70(10)	5706.15(17)	6208.75(18)	6172.1(2)	
<i>Z</i>	4	2	4	4	4	
<i>ρ</i> <sub>calcd</sub> [g cm <sup>-3</sup> ]	1.804	1.764	1.681	1.836	1.662	
<i>μ</i> [mm <sup>-1</sup> ]	1.599	1.550	1.396	1.408	1.380	
crystal size	0.19 × 0.16 × 0.09	0.40 × 0.12 × 0.05	0.22 × 0.11 × 0.10	0.18 × 0.07 × 0.06	0.18 × 0.11 × 0.08	
<i>θ</i> limits [°]	2.27 to 27.54	1.65 to 27.48	3.16 to 27.47	3.08 to 26.37	3.64 to 25.37	
<i>h</i> range	−9 to 14	−14 to 15	−13 to 14	−15 to 14	−13 to 12	
<i>k</i> range	−15 to 15	−23 to 22	−21 to 25	−25 to 24	−25 to 25	
<i>l</i> range	−41 to 41	−15 to 16	−32 to 32	−31 to 31	−31 to 31	
reflns collected	27802	25132	46916	63118	76285	
independent reflns	10239	10548	12996	12642	11292	
data/restraints/	10239/0/624	10548/1/623	12996/0/707	12642/0/806	11292/0/730	
parameters						
goodness-of-fit on <i>F</i> <sup>2</sup>	1.123	1.109	1.033	1.041	1.099	
<i>R</i> 1 <sup>[a]</sup>	0.0702	0.0317	0.0292	0.0424	0.0421	
<i>wR</i> 2 <sup>[a]</sup>	0.1768	0.0688	0.0565	0.0871	0.0915	
weighting scheme	<i>x</i> = 0.0488 <i>y</i> = 85.0794	<i>x</i> = 0.0467 <i>y</i> = 0.0000	<i>x</i> = 0.0256 <i>y</i> = 1.4306	<i>x</i> = 0.0358 <i>y</i> = 14.3902	<i>x</i> = 0.0302 <i>y</i> = 21.7512	
largest diff. peak/ hole [e Å <sup>-3</sup> ]	1.488/−1.898	0.683/−1.402	0.869/−0.586	1.390/−1.427	1.523/−1.335	
Flack parameter	0.14(6)	−0.02(2)	−0.021(15)	−0.03(2)	−	

[a]  $I \geq 2\sigma(I)$ ,  $w = 1/[\sigma^2(F_o^2) + (xP)^2 + yP]$ ,  $P = (Fo^2 + 2Fc^2)/3$ .

**12** in [D<sub>8</sub>]toluene. The NMR tube was pressurised with H<sub>2</sub> (20 bar) and was stored in its safety device at ambient temperature between the NMR measurements.

**Parahydrogen experiments:** A 52% para-enriched hydrogen mixture was obtained by filling a glass spiral full of activated carbon with normal hydrogen (pressure = 1.2 bar) in a liquid nitrogen bath (77 K) for 30 min. The parahydrogenation experiments were carried out in NMR tubes with Young Teflon valves (5 mm o.d.). An aliquot of a solution of **12** (0.5 mL, 1.2 mM) in a [D<sub>8</sub>]toluene/[D<sub>6</sub>]ethanol mixture (1:1) was prepared. The solution was deoxygenated, then filled with parahydrogen (4.5 bar) at room temperature and finally the tube was shaken thoroughly for 30 s, after which it was placed in the NMR probe. Then single scan <sup>1</sup>H or <sup>31</sup>P NMR spectra were acquired.

Several experiments by using [H<sub>2</sub>Ru<sub>4</sub>(CO)<sub>10</sub>(μ-1,2-**2a**)] (**12**) as a parahydrogenation catalyst were carried out in a mixture of [D<sub>8</sub>]toluene/[D<sub>6</sub>]ethanol (1:1). (*E*)-2-Methyl-2-butenic acid (tiglic acid) (**24**) (31 mg, 0.31 mmol) was added to a deoxygenated solution of **12** (1.2 mM, catalyst/substrate ≈ 1:500). The solution was then filled with parahydrogen (4.5 bar) at room temperature, shaken for 30 s and then introduced in the NMR magnet for single-scan <sup>1</sup>H NMR measurements.

**High-pressure IR spectroscopy:** All high-pressure infrared spectra were recorded with a Bruker Equinox 55 spectrometer by using the OPUS software program. The design, construction and mode of operation of the high-pressure infrared cell have been described earlier.<sup>[48]</sup> All spectra were collected by using Blackman-Harris 3-Term apodisation.

**X-ray structure determinations:** The crystals of clusters **4**, **7–9**, **12**, **13**, **15**, **17** and **19–21** were immersed in cryo-oil, mounted in a Nylon loop, and measured at a temperature of 100–120 K. The X-ray diffraction data were collected by means of a Nonius Kappa CCD diffractometer by using MoK<sub>α</sub> radiation (λ = 0.710 73 Å). The Denzo-Scalepack<sup>[49]</sup> or EvalCCD<sup>[50]</sup> program packages were used for cell refinements and data reductions. The structures were solved by direct methods by using SIR2002,<sup>[51]</sup> SIR2004<sup>[52]</sup> or SHELXS-97<sup>[53]</sup> with the WinGX<sup>[54]</sup> graphical user interface. A semi-empirical absorption correction (SADABS<sup>[55]</sup> or Xprep in the SHELXTL<sup>[56]</sup> program package) was applied to all data. Structural refinements were carried out by using SHELXL-97.<sup>[57]</sup> For cluster **13** the fluorine atoms F1 F2, F11 and F12 belonging to two of the CF<sub>3</sub> groups were disordered over two sites. F1 and F2 as well as F11 and F12 were refined with an effective standard deviation of 0.08 so that their U<sub>ij</sub> components approximated to isotropic behaviour. The hydride hydrogen atoms were either located from the difference Fourier map or placed on idealised positions by using the XHYDEX<sup>[58]</sup> program. Other hydrogen atoms were positioned geometrically and constrained to ride on their parent atoms, with C–H = 0.95–1.00 Å and U<sub>iso</sub> = 1.2–1.5 U<sub>eq</sub>(parent atom). The crystallographic details are summarised in Table 9. CCDC-876461 (**4**), 876462 (**7**), 876463 (**8**), 876464 (**9**), 652265 (**12**), 876465 (**13**), 876466 (**17**), 876467 (**19**), 876468 (**20**) and 876469 (**21**) contain the supplementary crystallographic data for this paper. These data can be obtained free of charge from The Cambridge Crystallographic Data Centre via [www.ccdc.cam.ac.uk/data\\_request/cif](http://www.ccdc.cam.ac.uk/data_request/cif).

## Acknowledgements

This paper is dedicated to the memory of Prof. John R. Moss, an inspiring colleague, mentor and friend, in recognition of his outstanding contributions to organometallic chemistry, including pioneering studies in cluster chemistry. The research has been sponsored by the Swedish Research Council (VR), the Swedish International Development Agency (SIDA), the South African National Research Foundation (NRF) and the Crafoord Foundation. We thank Prof. Roberto Gobetto for help and advice in the para-hydrogenation and HetCor NMR experiments. Furthermore, we thank Ahmed Fawzy Abdel-Magied and Anita Hoang for carrying out the catalyst recycling study. Finally, we thank Solvias AG, Basel, Switzerland, for generous gifts of samples of the ligands used in this investigation.

- [1] H. U. Blaser, F. Spindler, M. Studer, *Appl. Catal. A* **2001**, *221*, 119.
- [2] a) I. Ojima, N. Clos, C. Bastos, *Tetrahedron* **1989**, *45*, 6901; b) W. S. Knowles, R. Noyori, *Acc. Chem. Res.* **2007**, *40*, 1238; c) W. Li, G. Hou, X. Sun, G. Shang, W. Zhang, X. Zhang, *Pure Appl. Chem.* **2010**, *82*, 1429.
- [3] a) W. S. Knowles, *Angew. Chem.* **2002**, *114*, 2096; *Angew. Chem. Int. Ed.* **2002**, *41*, 1998; b) W. S. Knowles, *Acc. Chem. Res.* **1983**, *16*, 106.
- [4] a) M. J. Burk, M. F. Gross, J. P. Martinez, *J. Am. Chem. Soc.* **1995**, *117*, 9375; b) M. J. Burk, Y. M. Wang, J. R. Lee, *J. Am. Chem. Soc.* **1996**, *118*, 5142.
- [5] a) A. K. Smith, J. M. Basset, *J. Mol. Catal.* **1977**, *2*, 229; b) R. D. Adams, F. A. Cotton, *Catalysis by Di- and Polynuclear Metal Cluster Complexes*, Wiley-VCH, Weinheim **1998**; c) W. L. Gladfelter, K. J. Roessellet in *The Chemistry of Metal Cluster Complexes* (Eds.: D. F. Shriver, H. D. Kaesz, R. D. Adams), VCH, Weinheim **1990**, pp. 329–365; d) R. D. Adams, *Aldrichimica Acta* **2000**, *33*, 39; e) P. J. Dyson, *Coord. Chem. Rev.* **2004**, *248*, 2443.
- [6] G. Hogarth, S. E. Kabir, E. Nordlander, *Dalton Trans.* **2010**, *39*, 6153.
- [7] R. D. Adams, *J. Organomet. Chem.* **2000**, *600*, 1.
- [8] G. Süß-Fink, G. Herrmann, *J. Chem. Soc. Chem. Commun.* **1985**, 735.
- [9] G. Süß-Fink, *Angew. Chem.* **1982**, *94*, 72; *Angew. Chem. Int. Ed. Engl.* **1982**, *21*, 73.
- [10] G. Süß-Fink, G. Herrmann, *Angew. Chem.* **1986**, *98*, 568; *Angew. Chem. Int. Ed. Engl.* **1986**, *25*, 570.
- [11] M. W. Payne, D. L. Leussing, S. G. Shore, *J. Am. Chem. Soc.* **1987**, *109*, 617.
- [12] U. Matteoli, M. Bianchi, P. Frediani, F. Piacenti, C. Botteghi, M. Marchetti, *J. Organomet. Chem.* **1984**, *263*, 243.
- [13] M. Bianchi, G. Menchi, P. Frediani, U. Matteoli, F. Piacenti, *J. Organomet. Chem.* **1983**, *247*, 89.
- [14] a) C. Botteghi, S. Gladiali, M. Bianchi, U. Matteoli, P. Frediani, P. G. Vergamini, E. Benedetti, *J. Organomet. Chem.* **1977**, *140*, 221; b) U. Matteoli, V. Beghetto, A. Scriveranti, *J. Mol. Catal. A* **1996**, *109*, 45; c) U. Matteoli, G. Menchi, P. Frediani, M. Bianchi, F. Piacenti, *J. Organomet. Chem.* **1985**, *285*, 281; d) M. Bianchi, U. Matteoli, G. Menchi, F. Gloria, P. Frediani, F. Piacenti, C. Botteghi, *J. Organomet. Chem.* **1980**, *195*, 337.
- [15] P. Homanen, R. Persson, M. Haukka, T. A. Pakkanen, E. Nordlander, *Organometallics* **2000**, *19*, 5568.
- [16] P. Barbaro, C. Bianchini, G. Giambastiani, S. L. Parisel, *Coord. Chem. Rev.* **2004**, *248*, 2131.
- [17] C. Godard, A. Ruiz, C. Claver, *Helv. Chim. Acta* **2006**, *89*, 1610.
- [18] a) H. U. Blaser, F. Spindler, *Top. Catal.* **1997**, *4*, 275; b) H. U. Blaser, B. Pugin, F. Spindler, M. Thommen, *Acc. Chem. Res.* **2007**, *40*, 1240.
- [19] a) T. Sturm, L. Xiao, W. Weissensteiner, *Chimia* **2001**, *55*, 688; b) T. Sturm, W. Weissensteiner, F. Spindler, *Adv. Synth. Catal.* **2003**, *345*, 160.
- [20] V. Moberg, M. Haukka, I. O. Koshevoy, R. Ortiz, E. Nordlander, *Organometallics* **2007**, *26*, 4090.
- [21] V. Moberg, P. Homanen, S. Selva, R. Persson, M. Haukka, T. A. Pakkanen, M. Monari, E. Nordlander, *Dalton Trans.* **2006**, 279.
- [22] D. Braga, U. Matteoli, P. Sabatino, A. Scriveranti, *J. Chem. Soc. Dalton Trans.* **1995**, 419.
- [23] S. P. Tunik, T. S. Pilyugina, I. O. Koshevoy, S. I. Selivanov, M. Haukka, T. A. Pakkanen, *Organometallics* **2004**, *23*, 568.
- [24] M. R. Churchill, R. L. Lashewycz, J. R. Shapley, *Inorg. Chem.* **1980**, *19*, 1277.
- [25] R. D. Wilson, S. M. Wu, R. A. Love, R. Bau, *Inorg. Chem.* **1978**, *17*, 1271.
- [26] A. U. Härkönen, M. Ahlgrén, T. A. Pakkanen, J. Pursiainen, *J. Organomet. Chem.* **1997**, *530*, 191.
- [27] M. G. Ballinas-López, E. V. García-Báez, M. J. Rosales-Hoz, *Polyhedron* **2003**, *22*, 3403.
- [28] F. Barrière, R. U. Kirss, W. E. Geiger, *Organometallics* **2005**, *24*, 48, and references therein.

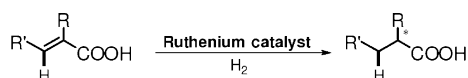
- [29] J. Nijhoff, M. J. Bakker, F. Hartl, G. Freeman, S. L. Ingham, B. F. G. Johnson, *J. Chem. Soc. Dalton Trans.* **1998**, 2625.
- [30] W. S. Knowles, *Acc. Chem. Res.* **1983**, *16*, 106.
- [31] M. T. Ashby, J. Halpern, *J. Am. Chem. Soc.* **1991**, *113*, 589.
- [32] a) R. Noyori, M. Ohta, Y. Hsiao, M. Kitamura, *J. Am. Chem. Soc.* **1986**, *108*, 7117; b) M. Kitamura, Y. Hsiao, R. Noyori, H. Takaya, *Tetrahedron Lett.* **1987**, *28*, 4829; c) M. Kitamura, Y. Hsiao, M. Ohta, H. Tsukamoto, T. Ohta, H. Takaya, R. Noyori, *J. Org. Chem.* **1994**, *59*, 297.
- [33] H. Zhang, C.-B. Yang, Y.-Y. Li, Z.-R. Donga, J.-X. Gao, H. Nakamura, K. Murata, T. Ikariya, *Chem. Commun.* **2003**, 142.
- [34] a) J. Collin, C. Jossart, G. Balavoine, *Organometallics* **1986**, *5*, 203; b) L. Vieille-Petit, G. Süß-Finke, B. Therrien, T. R. Ward, H. Stoeckli-Evans, G. Labat, L. Karmazin-Brelot, A. Neels, T. Buerger, R. G. Finke, C. M. Hagen, *Organometallics* **2005**, *24*, 6104.
- [35] C. M. Hagen, L. Vieille-Petit, G. Laurenczy, G. Süß-Finke, R. G. Finke, *Organometallics* **2005**, *24*, 1819.
- [36] L. N. Lewis, *J. Am. Chem. Soc.* **1986**, *108*, 743.
- [37] J. G. De Vries, *Dalton Trans.* **2006**, 421.
- [38] a) J. A. Widegren, R. G. Finke, *J. Mol. Catal. A* **2003**, *198*, 317; b) J. A. Widegren, M. A. Bennett, R. G. Finke, *J. Am. Chem. Soc.* **2003**, *125*, 10301.
- [39] T. Ohta, H. Takaya, R. Noyori, *Inorg. Chem.* **1988**, *27*, 566.
- [40] a) S. B. Duckett, C. L. Newell, R. Eisenberg, *J. Am. Chem. Soc.* **1994**, *116*, 10548; b) T. C. Eischenschmid, R. U. Kirss, P. P. Deutsch, S. I. Hommeltoft, R. Eisenberg, J. Bargon, R. G. Lawler, A. L. Balch, *J. Am. Chem. Soc.* **1987**, *109*, 8089; c) J. Natterer, J. Bargon, *Prog. Nucl. Magn. Reson. Spectrosc.* **1997**, *31*, 293; d) S. B. Duckett, C. J. Sleight, *Prog. Nucl. Magn. Reson. Spectrosc.* **1999**, *34*, 71.
- [41] a) R. Gobetto, L. Milone, F. Reineri, L. Salassa, A. Viale, E. Rosenberg, *Organometallics* **2002**, *21*, 1919; b) S. Aime, W. Dastrù, R. Gobetto, F. Reineri, A. Russo, A. Viale, *Organometallics* **2001**, *20*, 2924; c) S. Aime, W. Dastrù, R. Gobetto, A. Russo, A. Viale, D. Canet, *J. Phys. Chem. A* **1999**, *103*, 9702; d) S. Aime, R. Gobetto, D. Canet, *J. Am. Chem. Soc.* **1998**, *120*, 6770; e) D. Blazina, S. B. Duckett, P. J. Dyson, J. A. B. Lohman, *Angew. Chem.* **2001**, *113*, 3992; *Angew. Chem. Int. Ed.* **2001**, *40*, 3874; f) D. Blazina, S. B. Duckett, P. J. Dyson, J. A. B. Lohman, *Chem. Eur. J.* **2003**, *9*, 1045; g) D. Blazina, S. B. Duckett, P. J. Dyson, J. A. B. Lohman, *Dalton Trans.* **2004**, 2108.
- [42] a) I. T. Horváth, J. M. Millar, *Chem. Rev.* **1991**, *91*, 1339; b) A. Cusanelli, U. Frey, D. T. Richens, A. E. Merbach, *J. Am. Chem. Soc.* **1996**, *118*, 5265.
- [43] Y. Doi, K. Koshizuka, T. Keii, *Inorg. Chem.* **1982**, *21*, 2732.
- [44] J. L. Graff, M. S. Wrighton, *J. Am. Chem. Soc.* **1980**, *102*, 2123 and references therein.
- [45] M. I. Bruce, M. L. Williams, *Inorg. Synth.* **1989**, *26*, 262.
- [46] E. Tyrell, M. W. H. Tsang, G. A. Skinner, J. Fawcett, *Tetrahedron* **1996**, *52*, 9841.
- [47] J. Jeener, B. H. Meier, P. Bachmann, R. R. Ernst, *J. Chem. Phys.* **1979**, *71*, 4546.
- [48] W. Rigby, R. Whyman, K. Wilding, *J. Phys. E* **1970**, *3*, 572.
- [49] Z. Otwinowski, W. Minor, *Methods Enzymol.* **1997**, *276*, 307.
- [50] A. J. M. Duisenberg, L. M. J. Kroon-Batenburg, A. M. M. Schreurs, *J. Appl. Crystallogr.* **2003**, *36*, 220.
- [51] M. C. Burla, M. Camalli, B. Carrozzini, G. L. Casciarano, C. Giacovazzo, G. Polidori, R. Spagna, *J. Appl. Crystallogr.* **2003**, *36*, 1103.
- [52] M. C. Burla, M. Camalli, B. Carrozzini, G. L. Casciarano, C. Giacovazzo, G. Polidori, R. Spagna, *J. Appl. Crystallogr.* **2005**, *38*, 381.
- [53] SHELXS-97, Program for Crystal Structure Determination, G. M. Sheldrick, University of Göttingen, Göttingen (Germany), **1997**.
- [54] L. J. Farrugia, *J. Appl. Crystallogr.* **1999**, *32*, 837.
- [55] SADABS, Bruker Nonius scaling and absorption correction, v 2.10, G. M. Sheldrick, Bruker AXS, Inc., Madison, Wisconsin, **2003**.
- [56] SHELXTL, Bruker Analytical X-ray Systems, G. M. Sheldrick, Bruker AXS, Inc., Madison, Wisconsin, **2005**.
- [57] SHELXL-97, Program for Crystal Structure Refinement, G. M. Sheldrick, University of Göttingen, Göttingen (Germany), **1997**.
- [58] A. G. J. Orpen, *J. Chem. Soc. Dalton Trans.* **1980**, 2509.

Received: February 25, 2012  
Published online: ■ ■ ■, 0000

**Asymmetric Catalysis**

V. Moberg, R. Duquesne, S. Contaldi,  
O. Röhrs, J. Nachtigall, L. Damoense,  
A. T. Hutton, M. Green, M. Monari,  
D. Santelia, M. Haukka,  
E. Nordlander\* ..... ■■■■-■■■■

 **Efficient Cluster-Based Catalysts for Asymmetric Hydrogenation of  $\alpha$ -Unsaturated Carboxylic Acids**



**Cluster catalysis:** New clusters of the type  $[H_4Ru_4(CO)_{10}(\mu-1,2-P-P)]$ ,  $[H_4Ru_4(CO)_{10}(1,1-P-P)]$  and  $[H_4Ru_4(CO)_{11}(P-P)]$  (P-P = chiral diphosphine) have been synthesised and investigated as catalysts/catalyst

precursors for hydrogenation of  $\alpha$ -unsaturated carboxylic acids (see scheme). The cluster-based catalytic systems give excellent conversion rates and product selectivities, as well as good enantioselectivities.